Carbon 252 (2026) 121365

Contents lists available at ScienceDirect

Carbon

journal homepage: www.elsevier.com/locate/carbon

Colloidal dispersions of substrate-free gas-phase synthesized graphene: dispersion formulation for thin film formation

Lars Grebener [a], Yasaman Jarrahizadeh [b], Shaghayegh Pourdahrany [c], Muhammad Ali [d], Nicholas D. Wilson [e], Oliver Altenhoff [b], Stuart Goldie [e], Marika Schleberger [b,f], Axel Lorke [b,f], William Wong [c], Hartmut Wiggers [d,f], Michael A. Pope [e], Mohaned Hammad [a], Doris Segets [a,f,*]

[a] Institute for Energy and Material Processes – Particle Science and Technology, University Duisburg-Essen, Duisburg/DE, Germany
[b] Faculty of Physics – Experimental Physics, University Duisburg-Essen, Duisburg/DE, Germany
[c] Waterloo Institute for Nanotechnology (WIN) – Department of Electrical and Computer Engineering, University of Waterloo, Waterloo/CA, Canada
[d] Institute for Combustion and Gas Dynamics – Reactive Fluids, University Duisburg-Essen, Duisburg/DE, Germany
[e] Waterloo Institute for Nanotechnology (WIN) – Department of Chemical Engineering, University of Waterloo, Waterloo/CA, Canada
[f] CENIDE – Center for Nanointegration, Duisburg-Essen/DE, Germany

ARTICLE INFO

Keywords:
Gas-phase synthesized graphene
Analytical centrifugation
Dispersion formulation
Film formation
Hall effect conductivity

ABSTRACT

Substrate-free graphene synthesized in the gas-phase is a promising material with high specific surface area, exceptional purity, and conductivity. Despite these desirable properties for various applications, the transformation from the powder to stable dispersions and functional thin films remains an obstacle for the technical integration of this material. In this work, this challenge is addressed through systematic dispersion, stabilization, and thin film formation studies. Space- and time-resolved analytical centrifugation was used as an in-situ method to quantify the sedimentation of graphene. Remarkable stability was achieved only when agglomeration of graphene particles was suppressed in either solvents such as N-(2-hydroxyethyl)-2-pyrrolidone, a non-toxic analog to N-methyl-2-pyrrolidone or using polymers and surfactants as stabilizers like carboxymethyl cellulose, polyvinylpyrrolidone, and N-didodecyldimethyl-ammonium bromide in aqueous dispersions. These optimized dispersions were used to fabricate thin films via Langmuir deposition, spray coating and ink-jet printing. Hall effect conductivity measurements in van der Pauw geometry, novel to this class of thin films, and surface analysis revealed conductive, yet rough and porous layers formed by spray coating (mobility up to $\approx 2\ cm^2/V\bullet s$, carrier density $\approx 50\bullet10^{14}\ 1/cm^2$) and compact micro-rough layers by Langmuir deposition (mobility $\approx 19\ cm^2/V\bullet s$). This study provides insights into dispersion-process-structure-functionality relations and forms the framework for scalable dispersion formulation and thin film formation. The findings gained address major challenges for the device-integration of free-standing graphene for catalytic, adsorption and electronic applications.

1. Introduction

Since the first exfoliation of graphene by Novoselov et al. [1] (Nobel Prize 2010), much attention and research have been focused on this new class of materials. Its large tensile strength, thermal and electrical conductivity and specific surface area are desirable properties for numerous applications such as electronic, optical, and electrochemical devices. To utilize the promising properties of graphene and few-layer graphene (flG), different approaches have been studied extensively to produce colloidal dispersions of flG which could be processed further to devices by coating and printing methods [2–5]. One method is a top-down approach to exfoliate graphite directly in a liquid to produce flG dispersions. Another method involves the oxidation of graphite e.g. by modified Hummer's method [6] resulting in graphite oxide which can be exfoliated to graphene oxide (GO) thermally or in liquids that is functionalized with organic oxygen groups [7–16]. Since the disruption of the 2D lattice and chemical alterations degrade the desirable high electrical conductivity, GO is reduced by different means for instance

* Corresponding author. Institute for Energy and Material Processes – Particle Science and Technology, University Duisburg-Essen, Duisburg/DE, Germany.
E-mail address: doris.segets@uni-due.de (D. Segets).

https://doi.org/10.1016/j.carbon.2026.121365
Received 24 November 2025; Received in revised form 10 February 2026; Accepted 10 February 2026
Available online 11 February 2026

chemically by hydrazine or hydrogen, or by thermal decomposition to produce so called reduced graphene oxide (rGO) to restore some of the conductivity [16–24]. Alternatively, flG can be synthesized from small molecules like ethanol in the gas-phase using a microwave plasma and collected as a dry powder. This method yields high purity substrate-free crumpled 2D flakes: gas-phase synthesized graphene (gpG) [25].

Due to the high conductivity and large accessible surface area caused by their flat two-dimensional geometry, flG flakes are of interest for a number of applications, e.g., sensors, heterogenous catalysis, energy storage, electromagnetic shielding and (opto-)electronic devices. The deposition methods used include vacuum filtration onto porous substrates for free standing films (often several tens of micrometers thick), as well as 3D printing, blade coating, screen-printing, Langmuir deposition, or simply painting or drop-casting [10,18,26–39]. Specifically, gpG as a material has been used to produce silicon-graphene composites for the application in lithium-ion batteries [25].

However, despite many possible applications requiring a coating or printing step for which the flG must be prepared as a stable dispersion in a proper liquid, the transition of gpG from the powder to a device remains an unsolved challenge to date. The reason is that unlike the voluminous spherical composites (e.g. with Si) that seem to be compatible with a wider range of liquids, pure gpG is difficult to disperse in most common liquids. This is amplified by the absence of functional groups which could support interactions with liquids and stabilizers. There is a lack of understanding and empirical knowledge on the mechanism to stabilize the anisotropic particles while fulfilling basic technological demands to the dispersions: favorable drying behavior, compatibility of non-volatile compounds with the desired application and preferably non-hazardous substances. This is an obstacle which needs to be overcome in order to fully use the promising properties of gpG.

Most of the current knowledge on dispersions of flG is from the exfoliation of graphite, which directly yields flG dispersions. To increase the yield and quality of the flakes, different experimental routes have been explored. One strategy is to exfoliate in pure liquids such as N-methyl-2-pyrrolidone (NMP), dimethyl formamide (DMF), o-dichloro benzene (DCB) and chloroform (TCM), ionic liquids or even more volatile liquids such as isopropanol [13,40–50]. Other strategies include the use of stabilizers such as surfactants or polymers in less favorable liquids like water, and also electrochemical intercalation [27,31,51–59]. In this approach, graphite, liquids, and possibly additives like stabilizers and intercalation compounds are mixed and (shear) forces by sonification or other means are applied to the dispersion. In a consecutive step, sedimentation by gravity or centrifugation is used to separate larger aggregates and residual graphite. While this may be necessary to ensure a high quality and uniformity of the flakes, about 90 % of the particles or possibly more are discarded by estimate. Hence the yield is often very limited [4], which is not the case for gpG dispersions since the fabrication of the flakes and the dispersion formulations are independent from each other.

The quality of colloidal graphene dispersions, which can be defined as limited aggregation and sedimentation by gravity within a reasonable time period [3], has been evaluated by various methods: visual inspection after some time (shelf life time) [14,18,24,30], light scattering [60], zeta-potential evaluation [6,12,23,26], absorption in UV-Vis light after shelf time and determination of graphene concentration e.g. after varying centrifugation time and acceleration [16,49,51,61]. The dispersibility and liquid-phase exfoliation success in the means of flG concentration have been explored with surface energy, Hildebrand parameters and Hansen parameters by Hernandez et al. [62]. By comparing different concentrations – measured by UV-Vis spectroscopy – they report favorable parameters of about 40 mJ/m^2 for surface energy and Hansen parameters of δ_D 18 MPa$^{1/2}$, δ_P 9.3 MPa$^{1/2}$ and δ_H 7.7 MPa$^{1/2}$ for disperse, polar and hydrogen interactions respectively. This confirms the preference of flG for polar aprotic solvents with maximum concentrations of about 4 to 8 μg/mL like NMP, DCB and DMF, while demonstrating that other solvents can be used, too [62], e.g. to tune exfoliation by Hansen parameters [63]. These general trends have been reported for GO and rGO as well [16].

However, the determination of graphene concentration as a criterion for successful exfoliation and dispersion formulation suffers from the problem that the Lambert-Beer absorption coefficient is not constant [4], probably due to varying flake thickness, state of oxidation and conformation (flat sheet vs. crumpled). On review, coefficients from 66 to 13.6 cm^2/mg have been used to calculate the dispersion concentration from UV-vis absorption [4], thus the precision of the reported concentrations may be optimistic in some cases. This limits the validity of argumentations based solely on changes in concentration after exfoliation and centrifugation when comparing between different reports. Considerable progress towards more precise particle characterization methods has been achieved more recently by Walter et al. [64] on the basis of very dilute aqueous GO dispersion, by Goldie et al. [65] for different 2D materials such as WS_2 and flG, and by Sims et al. [66] for flG. The different studies have the common goal to improve the separation process for the selective centrifugation after exfoliation to obtain a narrow particle size distribution.

In this study, however, centrifugation will be used for a new perspective on graphene dispersions. While in the case of graphene preparation, it is a step to purify exfoliated graphene, in the case of gpG, it can be applied as a tool for characterizing dispersions as well. Analytical centrifugation (AC) is a versatile method in which the absorption of light is measured, space- and time-resolved, during accelerated sedimentation. This adds an in-situ perspective to the topic of graphene dispersions. Being space- and time-resolved, AC can take optical heterogeneity into account, be them in the spatial or time dimension and conclusions can be drawn on the progression of the sedimentation over the whole length of a measurement cell. Therefore, AC is a promising tool for the evaluation of the quality of colloidal graphene dispersions [67–69]. As the method allows for rapid dispersion characterization of a new material such as gpG in several different formulations, the above-mentioned lack of empirical knowledge and understanding of gpG dispersions are addressed, enabling to assess the stability of graphene dispersions in concentrations ready-to use for coatings. This is supported by previous results made in the past on other materials like carbon black [70,71]. Noteworthy, related methods have been applied by Park et al. [72] to compare chemically modified GOs and their stability in water and ethylene glycol. They used, among other methods, transmission profiles to directly compare the different dispersions and draw conclusions on the particle behavior. Hence, with the help of characterization and coating methods known from other cases, gpG can be investigated such that the technical integration of this promising material is facilitated.

Here, the interactions of gpG dispersed in different organic probe liquids and water with selected additives are explored by AC with the aim to find and describe formulations for stable gpG dispersions. In a second step, the formulations found are used to create conductive films of graphene particles by methods well-known for nanoparticles and that enable coatings on device-relevant scales, including ultrasound supported spray coating, Langmuir films and ink-jet printing. This approach enables the identification of optimal dispersion conditions that lead to flake networks with improved conductivity and mobility and provides fundamental insight into the colloidal mechanisms governing gpG stability and thin film assembly.

2. Experimental

2.1. Materials and material characterization

Pure gpG was synthesized as described by Münzer et al. [25] with the same equipment and methods. A microwave supported plasma is started in a hydrogen-argon gas stream. Ethanol is injected into the plasma where it decomposes to form graphene which can be collected from the exit stream using an inline membrane filter. Thus, this substrate-free material

is synthesized from a small molecule instead of exfoliation from graphite. For characterization, transmission electron microscopy (TEM, Jeol JEM-2200FS), X-ray photoelectron spectroscopy (XPS, Versaprobe II by ULVAC-Phi), specific surface area measurements (Anton Paar Nova 800, multipoint BET method), Raman spectroscopy (custom-built, quasi-confocal geometry, 532 nm semiconductor laser, 500 μW, spot size of about 1 μm^2) and infrared spectroscopy (IR, Bruker IFS 66v/S in ATR mode) were performed. Chemicals for the dispersions are used as received from the vendors and listed in Table S 1 in the supplementary information (SI). The Hansen parameters (δ_D, δ_P, δ_H) were obtained from HSPiP software (version 5.3.06). For an additional comparison of the product quality, experiments with commercially available graphene-related particles have been performed with sulfur-doped graphene (No. 900528, batch 1003745018) and graphene (No. 900561, batch 1003660766) purchased from Sigma-Aldrich and used as received.

2.2. Preparation of dispersions in pure liquids

To prepare dispersions in pure liquids, gpG and the selected liquids were weighed into 15 mL centrifuge tubes with a total of 5 mL liquid and a concentration of 0.5 and 0.1 mg/mL respectively. The choice of constant volumetric concentration will ensure that the same surface area of graphene is surrounded by the same volume of liquid for comparison. The dispersions were first mixed by an IKA vortex 2 for about 10 s and then dispersed by mild probe sonication at ~11 W (Branson Model 550) for 5 min while being cooled in an ice bath, similar to the procedure described in Ref. [71] with limited sonication power and duration to prevent damage to the particles [73]. The resulting dispersions were analyzed immediately after preparation.

2.3. Preparation of dispersions with additives

The dispersions tested for the possible formation of gpG thin films for practical applications were not prepared by concentration, but by weight fractions as this approach is more convenient to handle. Therefore, 0.1 wt% was used for graphene with the addition of different amounts of additives. The rest was filled up with the respective liquid to yield a total mass of 5 g. The mixing and dispersing of the components were performed as described above. The formulations are listed in Table 1, the additives in Table S 2.

Table 1
Formulations of dispersions for applications.

Name	Graphene	Additives		Liquids	
	wt%		wt%		wt%
CMC1.0	0.10	CMC	1.00	Water	rest
PAA1.0	0.10	PAA	1.00	Water	rest
PVP1.0	0.10	PVP	1.00	Water	rest
PAA0.9+CMC0.1	0.10	PAA	0.90	Water	rest
		CMC	0.10		
PVP0.9+CMC0.1	0.10	PVP	0.90	Water	rest
		CMC	0.10		
CMC0.1	0.10	CMC	0.10	Water	rest
PVP0.09+CMC0.01	0.10	PVP	0.09	Water	rest
		CMC	0.01		
Water	0.10	-	-	Water	rest
HEP	0.10	-	-	HEP	rest
NMP1.0	0.10	-	-	NMP	1
				Water	rest
NMP10	0.10	-	-	NMP	10
				Water	rest
DCB	0.10	-	-	DCB	rest
DCE	0.10	-	-	DCE	rest
TMC	0.10	-	-	TCM	rest
OSA0.1	0.10	OSA	0.10	Water	rest
TMOA0.1	0.10	TMOA	0.10	Water	rest
DDDA0.1	0.10	DDDA	0.10	Water	rest
SDS0.1	0.10	SDS	0.10	Water	rest
SBS0.1	0.10	SBS	0.10	Water	rest

2.4. Dispersion characterization

The dispersions of gpG were characterized by analytical centrifugation (AC, LUMiSizer 6514-44, LUM GmbH). The centrifuge was operated at 2000 rpm, corresponding to a g-force of about 575, and it continuously measured transmission profiles on a minimal time resolution of about 5 s. Thus, a space- and time-resolved transmission profile can be obtained and further evaluated as described in the results section and in the references [67–69,74–81]. All centrifugations were performed at 15 °C (DMSO 25 °C) and using 2 mm cells made of polycarbonate (water and alcohols), glass (DCB, DCE, TCM), or polyamide (for other liquids). To determine the Hansen solubility parameter (HSP), where the "S" in case of particles has to be understood as similarity [82], EtOH, HEX, TOL, ACE, EAC, DMSO, NMP and DMF were used as probe liquids. The calculations for the HSPs were performed using HSPiP software with the HSPs of the liquids used as implemented in the software and listed in Table S 1. For ranking the liquids, the integral extinction was used which is calculated from the space- and time resolved AC transmission profiles as established before [74,78,79].

To interpret the AC data quantitatively, previous theoretical models describing the sedimentation of flake-like particles are considered. Walter et al. [64] as well as Goldie et al. [65] derived quantitative models to describe the sedimentation velocity of flat flake-like particles to be used in centrifugation. For both approaches, the Stokes sedimentation for spherical particles has been adopted for a new geometry of flat disks. From the balance of force on a particle in a centrifugal field a general differential equation for particle movement can be derived: $dr/dt = Sr\omega^2$, with r being the radius [m], t the sedimentation time [s], S the sedimentation (Svedberg) coefficient [s] and ω the angular frequency [1/s].

To derive S, further considerations on the geometry of the particles have been made. The results of those can be interpreted that both the diameter d [m] and the thickness h [m] of a flake will increase the sedimentation velocity dr/dt with: $S \propto h^{2/3} d^{4/3}$ derived by Walter et al. [64] and $S \propto hd$ by Goldie et al. [65]. Thus, the sedimentation of graphene is still a topic of ongoing research and fundamental questions on the relation of particle shape and sedimentation velocity are unanswered to this day.

In summary, small and flat flakes will sediment the slowest, large and thick flakes the fastest. However, this does not consider complications such as re-agglomeration or a change in conformation, like crumpling of the 2D-flakes to a more spherical form. Therefore, flake thickness or layer number cannot be directly derived from AC data in this work. Instead, in this study, the primary AC results, transmission, time and position, serve as the basis for the evaluation of the graphene dispersion quality.

Photographs and optical micrographs (Olympus BX51) were taken from dispersions in 2 mm quartz cells about one day after preparation. Additional atomic force microscopy (AFM, TOSCA 400, Anton Paar; equipped with Nanosensors' SSS-NCHR in tapping mode) and optical microscopy (Olympus BX51) were performed for selected dispersions drop-cast on polished silicon thermal oxide wafers. The wafers were prepared by careful cleaning in organic solvents (hexane, ethanol) and water, followed by turning the surface hydrophobic with 3-aminopropyl triethoxysilane (APTES, Sigma-Aldrich, 99 % purity). A droplet of gpG dispersion was placed by a Pasteur pipette on the hydrophobic wafer and blown off with compressed nitrogen after about 10 s, to minimize drying-induced agglomeration.

2.5. Coating preparation and characterization

Coating layers from selected dispersions were prepared on polished sapphire wafers (c-plane, polished, 10 by 10 mm, cleaned) using an ultrasound spray coater (Ultrasonic Systems Inc., Prism 400 Ultra-Coat) at a low flowrate of only 0.2 mL/min and a head speed of 50 mm/s for

15, 25 and 35 passes of the spray head over the sample. For each pass, the movement was rotated to form a cross pattern with a pause of 5 s. The heating plate directly below the substrate was set to 150 °C to account for the low thermal conductivity of the substrate, while avoiding oxidation of gpG at higher temperatures. Films with HEP labeled as *drop-cast* were prepared by simply placing the wafer on a hot-plate set to 150 °C and slowly placing about 0.5 mL of dispersion using a pipette on the top of the substrate, ensuring the liquid did not run off.

Graphene dispersed in DCE was used to prepare thin films by Langmuir coatings. The dispersion was prepared as described above and further diluted to 0.025 wt% with DCE. The substrates (polished sapphire) were submerged under a water film in a Teflon trough. With a syringe pump (0.05 mL/min) the dispersion was dropped slowly onto the water from a tube, such that the droplet spreads on the water surface but does not penetrate into the water. The gpG formed a three dimensional crumpled cohesive film at the water-air interface, unlike films by similar methods reported in the past [83]. The dispersion addition was continued – for the purpose of reproducibility – until the droplet could no longer spread due to the accumulation of material at the interface. This occurred after 0.006 mL/cm^2 volume dispersion per surface area of water. The water was then removed by a suction pump positioned behind barriers, allowing the graphene film to lower onto the wafer substrates. The specimens were dried at 40 °C.

Furthermore, graphene films were printed using an inkjet printer (CERAPRINTER F-Serie, Ceradrop) equipped with a Dimatix-Samba cartridge head. The ink formulation consisted of 0.1 wt% graphene dispersed in DCB. Jetting was carried out under stable conditions at a frequency of 10 Hz, yielding droplets with an average volume of ~7 pL and a velocity of 1.2 m/s. Silicon wafers with a thermally grown 100 nm SiO_2 layer were used as substrates. Prior to printing, the substrates underwent sequential solvent cleaning followed by UV-ozone treatment. Under these jetting parameters, the deposited droplets exhibited a splat diameter of approximately 55 μm on the cleaned substrate surface. The substrate was heated up to 50 °C during the printing.

Characterizations of the coating properties were performed to evaluate film morphology and electrical performance. Transmission optical microscopy (Olympus BX51), Raman spectroscopy (WITec alpha300 RA confocal Raman Spectrometer, 532 nm 1 mW laser, 1800 g/mm grating), AFM, scanning electron microscopy (SEM, FEI Helios 600 NanoLab DualBeam) and optical profilometry (S Neox 090 operated in confocal mode) were performed.

Furthermore, the electrical properties of the layers were investigated using Hall measurements in van der Pauw geometry to determine conductivity, carrier density and mobility. A schematic illustration of the electrical measurement setup, and a representative sample are provided in Figure S 1. In the measurement setup, the current was applied by a Keithley 2400 source meter, while voltages were measured using a Keithley 2000 digital multimeter. A perpendicular magnetic field of up to 1.2 T was generated using a Bruker B-E 10 electromagnet. All electrical measurements were performed using automated data acquisition and instrument control implemented in Python. Contacts, made of Ti/Au (5 nm/100 nm), were deposited by shadow-masked evaporation at the corners of the sample. They displayed ohmic behavior (Figure S 9a). Measurements were conducted at room temperature in the dark and in a vacuum environment to avoid interference from light, air or moisture. The sheet resistivity was calculated by applying the van der Pauw equation [84] to four-point resistance measurements performed between adjacent contact pairs, and the sheet conductivity was obtained as the inverse of the sheet resistivity. For the determination of Hall mobility, a constant current was applied to the sample, the transverse voltage was measured between diagonal contact pairs, and a magnetic field was applied perpendicular to the sample plane. Further details on resistance configurations, van der Pauw analysis, and Hall mobility evaluation are provided in the SI (pages 3 and 4). It is important to note that the classical van der Pauw technique assumes a uniform, continuous (hole-free) thin film with edge contacts, but it can be applied with care to samples that contain isolated holes or small voids. The van der Pauw measurements are therefore primarily used as a consistent, comparative metric across processing routes (spray coating vs. Langmuir deposition) and pass or layer counts. Samples with substantial void fractions or discontinuities (e.g., HEP coatings) fall outside the method's applicability and were not characterized by the van der Pauw method.

For evaluation of the electrical properties of the printed graphene, Cr/Au electrodes (5/40 nm) were thermally evaporated onto the Si/SiO_2 substrates with a 100 nm oxide layer and patterned via standard photolithography. The electrode pair consisted of two parallel contacts separated by 10 μm and each 1000 μm long. After metal deposition, the substrates were cleaned sequentially in deionized water, acetone, and isopropanol using sonication, followed by nitrogen drying. A brief UV–ozone treatment was then applied to remove residual organic contaminants. Graphene ink was inkjet-printed in the gap between the electrodes with multiple passes to ensure complete coverage. The printed samples were dried under vacuum overnight to remove remaining solvent, and current–voltage (I–V) measurements were carried out under vacuum and dark conditions.

3. Results and discussion

3.1. Particle characterization

The results of the characterization of gpG particles after the synthesis in gas-phase from ethanol are displayed in Fig. 1. TEM micrographs (Fig. 1a) and Raman spectroscopy (Fig. 1b) indicate that the flakes harvested from the microwave plasma reactor consist of flG. The full width at half maximum (FWHM) of the 2D signal is 68 cm^{-1} and the intensity ratio of $I_{2D}/I_G = 1.57$, both suggest an average of bi- and tri-layered graphene flakes. The wrinkled structure of the flakes (size 300 ± 100 nm) is typical for this material [85] and leads to defects on the edges of the flakes, as suggested by the ratio $I_D/I_G = 0.34$. This is a higher defect density as for most graphene exfoliated or synthesized on a substrate but has considerably less defects than many substrate-free flG flakes. The position of the D signal at 1580 cm^{-1} suggests the lattice is not significantly strained or doped. The purity of the flakes is supported by the chemical characterization with IR spectroscopy (Fig. 1c) and XPS (Fig. 1d). No significant peaks in the expected region for e.g., carbon-oxygen bonds can be found, thus, most oxygen – originated from ethanol in the synthesis – is not incorporated in the 2D lattice of this flG. By XPS, the oxygen content of gpG is below 1 at%. No contamination of soot-like spherical carbon can be found. The specific surface area as determined with the BET method is about 330 m^2/g.

3.2. Dispersions in pure liquids

3.2.1. General dispersion studies

The stability of gpG in liquid media determines its suitability for processing into coatings and films. To elucidate solvent–graphene interactions, AC was applied to evaluate the sedimentation behavior of gpG in a set of pure probe liquids with varying polarity and molecular structure.

As a first step to examine the dispersibility of gpG, dispersions of pure liquids with different chemical structures and consequently different intramolecular forces are used. The results of exemplary dispersions of 0.5 mg/L concentration are displayed in Fig. 2. On the left side, the transmission profiles are displayed. Here, the transmission through the measurement cell in the centrifuge vs. the position in the cell is shown, the position itself is with respect to the center of rotation. The meniscus is seen at just about 108 mm and the bottom of the measurement cell at about 127.5 mm, the dispersion is in between. The color-scale diagrams on the right side are called transmittograms [77]. Here, the space-time resolved sedimentation of gpG in dispersion is shown in a single diagram.

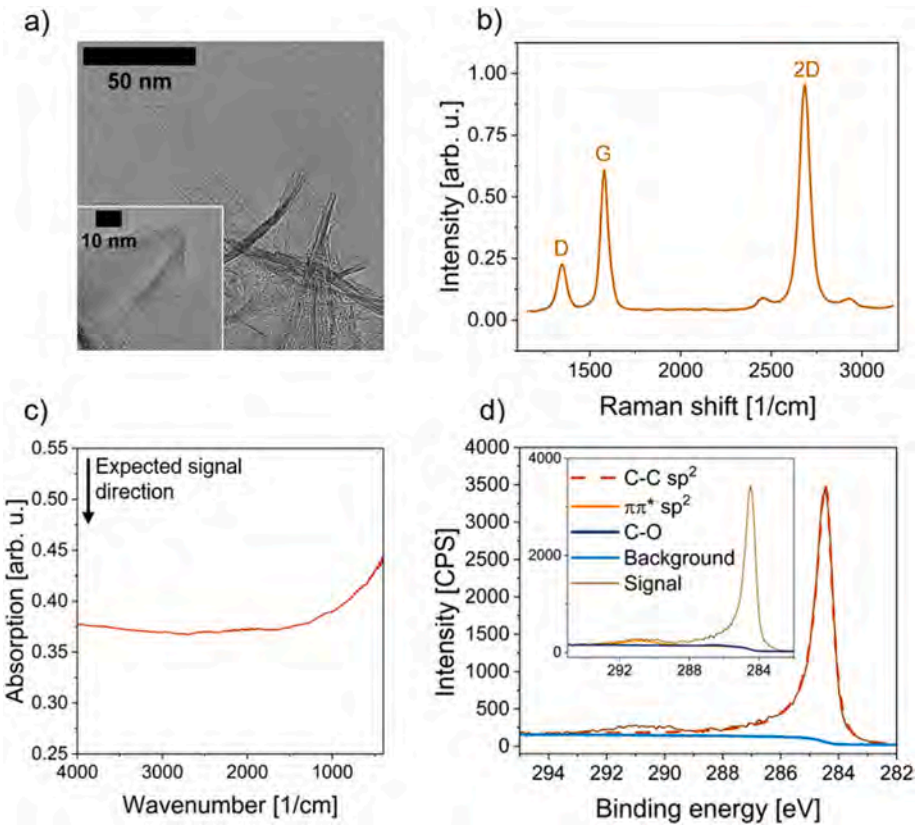

Fig. 1. Particle characterization of gpG synthesized from ethanol in the gas-phase. a) TEM micrographs of aggregated and separated flakes; b) Raman spectrum of dry powder, the intensity is normalized to the 2D signal; c) IR spectrum in the region where functional organic groups are to be expected; d) XPS detailed spectrum for the C1s binding energy, signal intensity in counts per second (CPS).

For ethanol (Fig. 2a and b), the sedimentation is fast and complete within 5 s. The large spikes in the transmission profile indicate gaps between the particles with clear liquid in between. The gpG in DMSO (c) seems to be more stable judging from the transmission profiles, yet the transmittogram (d) shows that much of the graphene sediments within the first 10 min. As for ethanol, the transmission profiles are approximately parallel to the abscissa, the transmission is about equal in the whole cell at a given point in time. This is in contrast to expectations. If the conditions defined by Walter and Goldie et al. [64,65] are met (constant shape and no agglomeration), a distinct sedimentation front would be observed, indicating polydisperse sedimentation or zone sedimentation as described by Lerche and Sobisch [81], and similarly for modified GO by Park et al. [72] with a transmission profile at an angle of about 20 to 90° towards the abscissa. The top liquid would clear up first, the bottom the latest, possibly with different fractions identifiable. Yet, in the case of ethanol and DMSO, it seems like sedimentation is progressing fast, much faster than the differences in density or the viscosity of the liquids would suggest. However, if the flake diameter is considered to be constant, this unexpected behavior can be explained as follows. When the flakes are agglomerating plane-on-plane instead of aligning edge by edge, then the observed increase in sedimentation velocity can be attributed to an increase in the effective flake thickness. This is consistent with both scaling relationships $S \propto h^{2/3}$ or $S \propto h$ and which predict a faster sedimentation when thickness increases due to agglomeration. This is furthermore consistent with Süß et al. [74], who found a similar agglomeration behavior for spherical carbon in different probe liquids. Altogether, this means the re-agglomeration is happening on very short timeframes of seconds and below and rather by plane-on-plane agglomeration and not in an edge-by-edge-configuration. This agglomeration seems to have progressed fast in case of ethanol (a) and the large spikes in the transmission profile are due to the agglomerates and the clear liquid in between.

DMF (Fig. 2e and f) and NMP (Fig. 2g and h) have been reported as two of the most favorable liquids for exfoliating graphene in liquid phase [2–4,6,13,44,49,56]. For dispersing gpG in these two liquids, this can be confirmed as well. In DMF, sedimentation and agglomeration are slowed down substantially, while in NMP both agglomeration and sedimentation are effectively suppressed. Therefore, if a dispersion with a high yield of graphene from exfoliation is achieved in past reports, it is likely due to both factors: (i) weakening the interlayer adherence of the graphene particles as well as (ii) suppressing the re-agglomeration during exfoliation and stabilizing the graphene flakes in dispersion during the consecutive centrifugation and separation. Both of which would explain the reportativity high concentration of graphene dispersions from liquid-phase exfoliation. In order to visualize these observations, photographs and micrographs of the dispersions in ordinary 2 mm quartz cells have been prepared and are presented in Figure S 2.

3.2.2. *Hansen solubility parameters*

After this first assessment, the dispersions' stability depending on the particle and the probe liquid can be compared directly by integrating the extinction over the length of the measurement cell to determine the HSPs. As can be seen in Fig. 3a, on a logarithmic timescale, dispersions with fast sedimentation can be distinguished well from more stable dispersions. Here, in the first 10 min of centrifugation, only NMP and DMF show no signs of sedimentation. Thus, only these two are to be considered good liquids in the sense of HSP studies. The results of this evaluation for the dispersions of 0.5 g/L are shown in Fig. 3b. The results of the dispersions prepared with 0.1 mg/L are not different in principle and therefore summarized in Figure S 3 in the SI.

The calculated HSPs of gpG ($\delta_D = 17.81$ MPa$^{1/2}$; $\delta_P = 12.84$ MPa$^{1/2}$; $\delta_H = 9.1$ MPa$^{1/2}$) in Fig. 3b demonstrate a strong tendency for polar and dispersive bonds. These bonds, with respect to the probe liquids applied

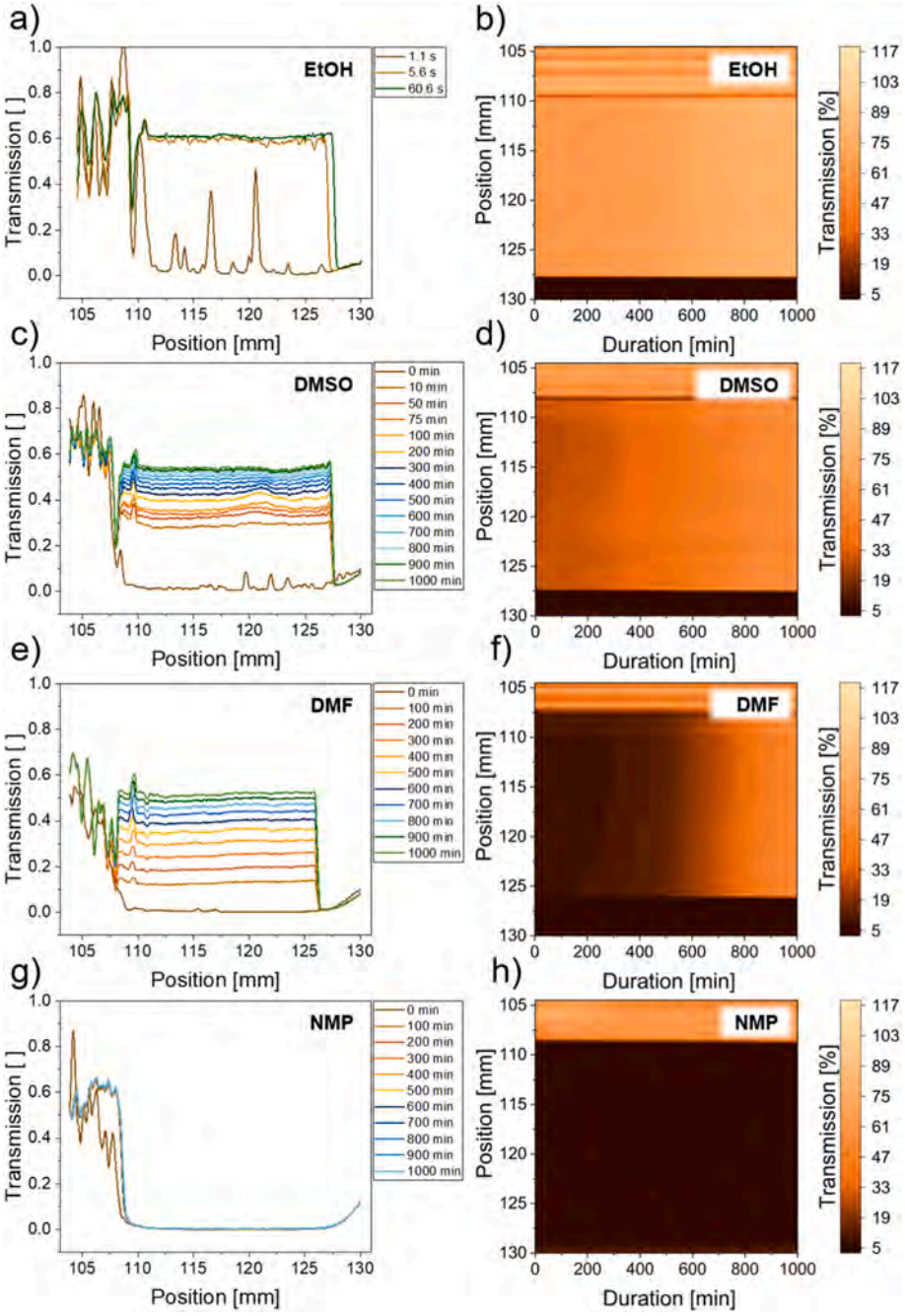

Fig. 2. Transmission profiles and transmittograms of selected dispersions of gpG in pure liquids with the concentration of 0.5 mg/mL. Panels a) and b) EtOH with the data cut in a) after 60.6 s due to complete sedimentation; c) and d) DMSO; e) and f) DMF; g) and h) NMP.

in this study, are generally created by liquids, which molecules have a permanent dipole in a system of π-electrons as well as non-polar saturated bonds. Hernandez et al. [62] reported rather similar parameters, but noteworthy with less tendency for polar bonds. Yet in their study, graphene was exfoliated from graphite in the probe liquid. In this scenario, not only the ability of a probe molecule to stabilize a dispersion is examined, but the result is superimposed with the probe liquid's ability to exfoliate the material under consideration. For a molecule to weaken the bonds between graphite layers, it needs to intercalate between these layers. Consequently, it is not only a thermodynamic process – as could be interpreted from HSPs – but also a kinetic since diffusion processes have to take place as well. Thus, one can conclude that the best molecular structure for exfoliation is limited to the best compromise to fulfill both requirements: diffusion and stabilization. This cannot be represented by HSPs alone, as they do not account for the size of a molecule but describe intermolecular interactions only. The results in Fig. 3 on the other hand reflect only the stabilization, since the gpG flakes do not require exfoliation but mild dispersing and therefore only the suppression of agglomeration is tested as described above in the discussion of Fig. 2.

Molecular dynamics simulations have been applied in the past to better understand the interactions of liquid molecules and the graphene surface. Similar preferences for solvents during exfoliation were found on the basis of solvent monolayers on the carbon surface of graphene or surfactant molecules hindering re-agglomeration [86,87], introducing energy barriers [58]. If the energy barrier by repulsive forces are not sufficient, agglomeration of graphene sheets happens plane-on-plane in the time period of some nanoseconds [86]. Goldie et al. [88] concluded

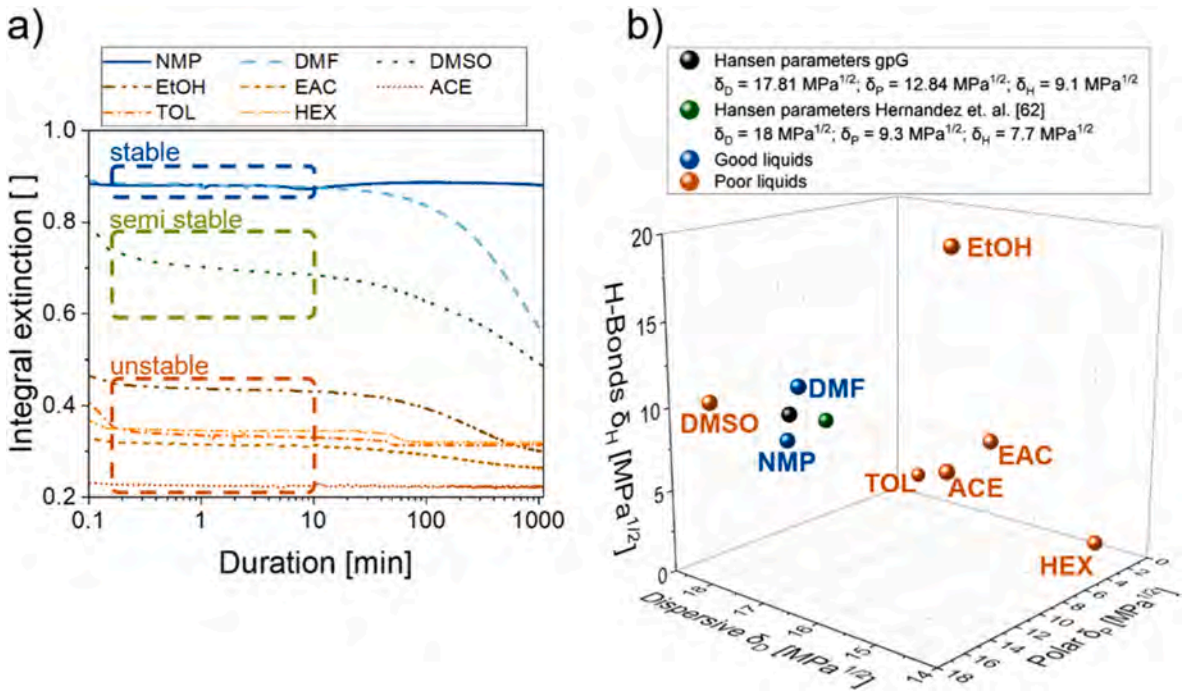

Fig. 3. Comparison of dispersibility of different probe liquids for gpG in dispersions of 0.5 mg/L. a) Evaluation by the integral extinction along the measurement cell; b) HSP for the applied probe liquids and graphene flakes.

that molecules with a π-electron system and a dipole moment along it which can adsorb well on the graphene surface and a group with saturated bonds can facilitate exfoliation by hindering the re-agglomeration. Probe molecules with a π-electron system and a dipole moment will orient aligned with the π-electrons of the graphene layer, the saturated group will face away from it, thus posing a steric hindrance. Interestingly, this is likely not only true for NMP and similar small molecule compounds, but also for e.g. surfactants. If a liquid does not have a conjugated π-electron system, no preferable orientation was to be found, even if a permanent dipole is present for instance in the case of ethanol. For DMSO, the dipole moment loosely aligns with the graphene plane, the free electrons and methyl groups facing opposite. Yet in general, DMSO as confirmed in this work is less favorable than NMP, possibly due to the stronger steric hindrance from the more strictly oriented NMP. Water, however, cannot offer any significant barrier. From these findings, it can be concluded that a small molecule such as a solvent to stabilize graphene in dispersion, should have *amphiphilic* properties in a sense that one side should be attractive towards the graphene plane with a strong dipolar moment, while the other should be repellant, e.g. with aliphatic hydrocarbons, creating an energy barrier between the sheets. This shifts the dynamic equilibrium of agglomerated-dispersed nanoparticles in the sense of Müller et al. [89] towards the dispersed gpG flakes in this study.

The agglomeration of the gpG can be derived from the transmission profiles and transmittograms indirectly. To possibly observe the agglomeration directly other imaging methods are required. Graphene dispersions have been drop-cast onto hydrophobic silicon thermal oxide wafers and blown off with compressed air before complete evaporation. Micrographs by AFM and optical microscopy have been recorded, and the results are presented in Figure S 4 in the SI. In summary, the micrographs show a trend to less agglomeration in the order of EtOH > DMF > NMP. However, the agglomeration cannot be suppressed completely by the preparation method.

Furthermore, TEM microscopy (Figure S 5) and additional AC experiments (Figure S 6) have been conducted with commercial flG and sulfur-doped flG. The results are discussed in the SI (page 6 and 7). In nuce, both materials are impurified with soot, the undoped flG more than the sulfur-doped flG, and both yield less stable dispersions than gpG. The results show, it is possible that the presence of soot destabilizes the dispersion further but that the wrinkled and folded structure of gpG increases the stability in solvents like NMP, which has been found by Luo et al. as well for rGOs [90].

3.3. Dispersions for the formation of thin films

3.3.1. Dispersions in pure liquids

After evaluating the sedimentation behavior of gpG dispersed in pure liquids, other dispersions for the practical use of the formation of thin films were prepared. For a dispersion of flG or gpG to be applied in a coating forming a dry layer, certain requirements can be formulated. First and foremost, the dispersion should be stable against sedimentation at least for the time required to complete the coating process. Yet, as seen above, to stabilize graphene in dispersion against sedimentation does necessarily mean to suppress the agglomeration in the first place. Therefore, the first task to formulate a dispersion of gpG is to separate the individual graphene flakes. Furthermore, it is generally desirable to use components which are not toxic and – in the case of liquids that must evaporate – have a low heat of evaporation and boiling point. The dispersion should be prepared with as little effort and time as possible. However, the fast-drying, volatile organic liquids such as EtOH and EAC do not yield sufficiently stable dispersions. NMP and DMF on the other hand would yield sufficiently stable dispersions, but both have other disadvantageous properties: toxic and high boiling point. The same intramolecular properties that are advantageous for adsorption on the graphene surfaces [88] seem to yield a high cohesive energy as well, which results in a high boiling point. To formulate dispersions which fulfill the desired properties, different approaches were followed and tested. The formulations and abbreviations are outlined in Table 1. In general, the abbreviations with numbers refer to the additive with a concentration in weight percentage (NMP10 is water with 10 wt% NMP) and the abbreviations without numbers refer to pure liquids.

Because the pure liquids used above did not satisfy all requirements simultaneously, a second step was taken using other liquids and water-based mixtures with selected additives. Water is desirable as it is not

hazardous and does not emit hydrocarbons during drying, with a moderate boiling point. Yet, pure water (Fig. 4a) does not yield stable dispersions, only a very small amount of gpG, as seen by the limited absorption, seems to be semi-stable and sediments until about 700 min. When NMP, which yields the most stable dispersions in the step before, is used as an additive in water with 1 wt% and 10 wt% (Fig. 4b and c), the stability is not increased, which demonstrated that NMP is not selectively adsorbing on the surface of gpG, unlike a surfactant eventually would.

For additive-free dispersions, HEP can serve as a non-toxic alternative to NMP. The chemical structure and physical properties are similar, yet HEP is not labeled as CMR (carcinogenic, mutagenic, and toxic to reproduction) and is not on the SVHC (substance of very high concern) list. However, for coatings, the high boiling point and slow evaporation remain challenging. More volatile solvents with similar polar bonds indicated by HSPs (in particular δ_p) can be found among chlorinated solvents. DCB and DCE (e and f) yield stable suspensions not indicating relevant sedimentation within 700 min centrifugation. Note, the different shape of the transmittograms is due to the use of glass cells, e.g., the line just above 125 mm corresponds to the glass bottom of the cell. TCM does not yield stable dispersions – in contrast to previous results like from O'Neill and Khan [45] for the exfoliation of graphite. This might be due to the weaker polar interaction (δ_p) or the lack of a repulsive part towards graphene within the trichloromethane molecule. The drawbacks of chlorinated solvents such as DCB and DCE are that these solvents corrode polymers which make them difficult to handle in

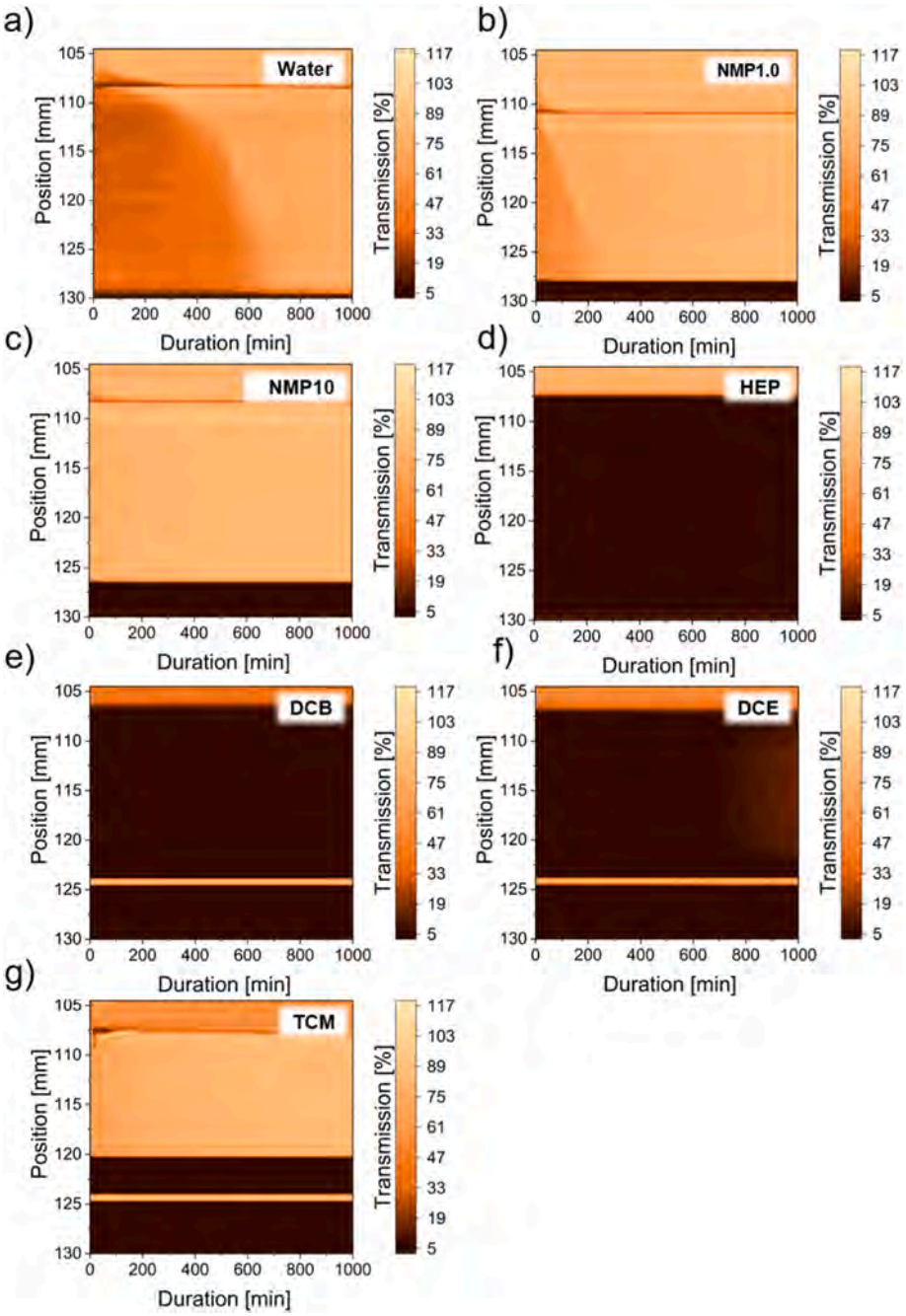

Fig. 4. Transmittograms for 0.1 wt% gpG in different liquids, centrifuged with a relative acceleration of about 575 g. a) Pure water; b) water with 1 wt% NMP; c) water with 10 wt% NMP; d) pure HEP as a non-toxic alternative to NMP; e) DCB; f) DCE; g) TCM. Note, the region of high transmission at about 125 mm in e-g) is due to the use of glass cells, the line just above 125 mm is the bottom of the cell.

coating machines, as well as their persistence and in case of DCE the toxicity as a CMR and SVHC substance.

The results of the other pure liquids HEP, DCB, DCE and TCM show that stable dispersions can be found beyond the small HSP volume close to DMF and NMP in Fig. 3b, as the HSPs of the other probe liquids are scattered also among liquids which yield unstable dispersions (comp. Table S 1). Therefore, it is not possible to predict the stability of a dispersion with gpG based on HSPs alone. To elaborate on this matter, different physical properties of each probe liquid are compiled in Table S 3 in the supplementary information. The liquids can be categorized for yielding stable (NMP, HEP, DCB), medium stable (DMF, DCE) and unstable dispersions with gpG. With this clustering and assuming NMP and HEP to have similar properties, it becomes apparent that there is no single physical property (like dipole moment or surface tension) nor related numerical property (like HSPs) which predicts if a dispersion is stable or not. However, it is possible to formulate a combination of properties for a probe liquid under which stability is to be expected: The dipole moment should be at least 2 D strong, the molecular volume should be about 100 mL/mol or higher, the molecule should be formed as a ring with one side consisting of apolar bonds. If one or more of these properties is not sufficient, a decrease in stability is to be expected. For instance, if the probe molecule does not have a ring structure with apolar bonds like DMF, the stability is decreased substantially. If the dipole moment is not sufficiently large, like for TOL, the stability is decreased. However, the proposed *amphiphilic* structure of probe molecules for stable dispersions cannot be presented by these numerical values directly, as the disperse HSP scatters too much, but only indirectly by the molecular structure and volume.

This interpretation is confirmed by theoretical approaches such as molecular dynamic simulations involving one or two graphene planes and the assemble of probe molecules. Shih et al. [86] concluded from such simulations that in order to stabilize a graphene dispersion, the interactions between the adsorbed monolayer of probe liquid molecules on the graphene plane should be strong. The stronger this interaction compared to the bulk interaction of the liquid is, the more is the agglomeration hindered, as the energy barrier which includes desorption is raised. As mentioned above, Goldie et al. [88] added that some probe molecules adopt to preferred orientations following the dipole moment of molecules such as NMP. However, if the dipole of such a molecule is oriented facing towards the graphene plane in accordance with the simulations, two graphene flakes would approach each other with a monolayer of molecules with opposing dipole moments, posing a repulsive force. Both of these studies point towards the formation of a strong and oriented monolayer of liquid molecules on the graphene plane. This interpretation is visualized in Figure S 7 by a sketch.

3.3.2. *Aqueous dispersions with additives*

To achieve stable aqueous dispersions, additives were therefore tested. Three different polymers were used, CMC, PAA, PVP. All of which are known as effective additives e.g. for GO and similar particles. Thus, the experimental focus is shifted towards the gpG. The first two polymers have anionic side-groups, the latter the same γ-lactam ring as NMP and HEP. The transmittograms are displayed in Fig. 5. With a concentration of 1 wt%, ten times larger than that of gpG, the dispersions can be stabilized well, following the order CMC > PVP > PAA. For all the samples, a polydisperse sedimentation can be identified, indicated by the inclination in the transmittograms. Thus, all three polymers suppress the agglomeration well. CMC is still effective at just 0.1 wt% and as mixtures with 0.9 wt% PAA or PVP, even further lowering the concentration to 0.01 wt% CMC and 0.09 wt% PVP was possible, while still retaining reasonable stability against sedimentation. This makes all three polymers potential additives for non-toxic gpG dispersions.

Interestingly, comparison of 1 wt% NMP (Fig. 4b) and 1 wt% PVP (Fig. 5d) addition to gpG in water shows that the stability of a dispersion is not determined by the attractive group towards graphene alone. As both are easily dissolved in water, their only difference is that NMP is a small molecule and PVP a polymer. If PVP or NMP adsorbs onto the particle surface replacing water molecules, it is possible that the adsorption of PVP opens more translational degrees of freedom in terms of molecular movement than NMP. This increases the entropy of the system, making PVP adsorption thermodynamically more favorable than that of NMP. This entropic effect likely contributes to the enhanced stability of PVP-stabilized dispersions similar to the improved stability of coordination compounds with ligands which have more than one bond to the central atom. However, this is an interpretation of the presented data. In any case, it is apparent that the actual stabilization is due to both Derjaguin–Landau–Verwey–Overbeek (DLVO) and non-DLVO mechanisms (e.g. maintaining osmotic pressure between the particles).

Not only can polymers be used to stabilize gpG in water, but also surfactants. Therefore, different surfactants have been tested which are like the polymers known as additives, and the results are shown in Fig. 6. OSA, SDS and SBS are similar anionic surfactants with a sulfonate or sulfate polar group. The apolar parts have different sizes with SDS being the largest and SBS the smallest. All anionic surfactants are well miscible with water (critical micelle concentration for SDS is about 2.3 mg/mL and for OSA about 30 mg/mL) [91], which are well above the approximate concentration used in this study (0.1 mg/mL). This concentration was chosen to minimize the possible impact of the non-volatile non-conductive surfactant salts on the final coatings. Cationic surfactants derived from quaternary ammonium have been tested, too. The critical micelle concentration is about 35 mg/mL for TMOA [92] and as small as about 0.032 mg/mL for DDDA [93]. Thus, the cationic surfactants are used both below and above their respective critical micelle concentration, with DDDA yielding a more stable dispersion than TMOA. The results suggest that surfactants with larger apolar parts in their molecular structure yield more stable dispersions, generally pointing towards the effect of steric hindrance as it was found for non-ionic surfactants in the exfoliation scenario, while for anionic surfactants the electrical double layer was found to be more dominant [58].

Generally, it is reported in literature that surfactants can support the exfoliation of graphene from graphite, with cholates being preferable over non-ionic, cationic surfactants, or other anionic surfactants like SDS [31,57,58]. In other cases of rGO at 0.1 mg/mL particle concentration with 0.05 and 0.5 wt% additive concentration, SDS was not found to be practical to stabilize the dispersion [94], which is in contrast to the findings in this study. In the same context, PVP showed to yield stable dispersions, which is in agreement to the results here. However, the dispersions were prepared at the extreme pH of 1 and 12 unlike in this study. It is therefore apparent again that the details in the preparations are important factors for the stabilization of graphene dispersions, be it the different flakes or the liquids and additives.

It is further noteworthy that the films Fernández-Merino et al. [94] produced from dispersions containing polymers and surfactants often exhibited lower conductivity, whereas samples with a higher rGO fraction (e.g., rGO in a pure liquid) showed the best electrical performance. This observation highlights the potential negative influence of stabilizing additives on graphene's electronic properties. Therefore, to evaluate the practical impact of stabilization on coating performance, selected dispersions were further processed into model coatings using Langmuir deposition, ultrasonic spray coating and ink-jet printing.

3.4. *Formation of conductive thin films*

3.4.1. *General aspects*

For the possible application of gpG in devices such as sensors or in energy storage, thin films are required that aim for fulfilling two quality demands: sufficient electrical or thermal conductivity and high surface area for some applications. To utilize the intrinsic properties of gpG, different thin films are prepared by Langmuir deposition, spray coating and ink-jet printing with selected dispersions. The different techniques were chosen as they are well-known for the deposition of particles onto a

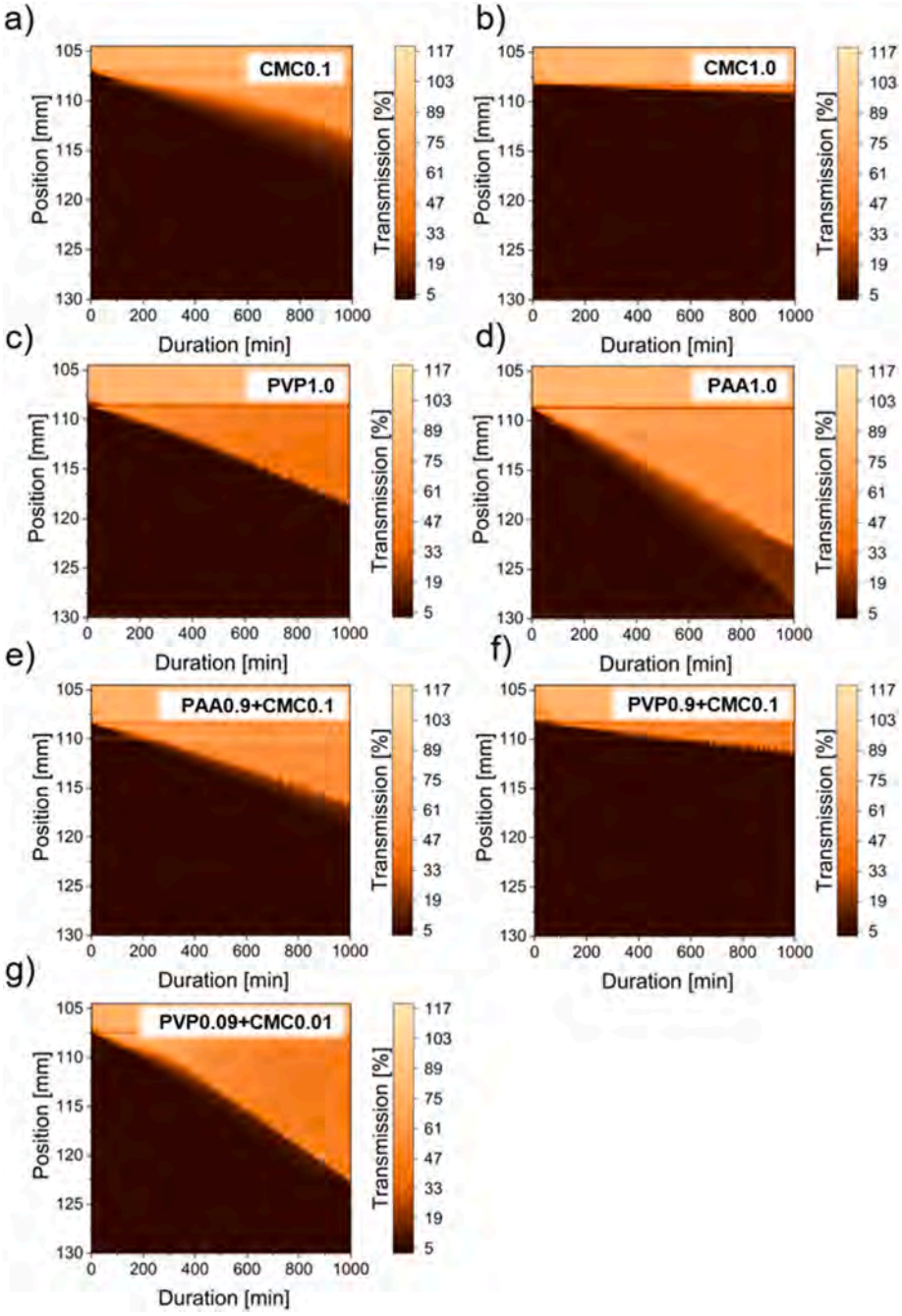

Fig. 5. Transmittograms for 0.1 wt% gpG in water with different polymers as additives centrifuged with a relative centrifugal acceleration of about 575 g. a) Water with 0.1 wt% CMC and b) with 1 wt% CMC; c) water with 1 wt% PVP; d) water with 1 wt% PAA; e) water with a mixture of 0.9 wt% PAA and 0.1 wt% CMC; f) water with 0.9 wt% PVP and 0.1 wt% CMC and g) with 0.09 wt% PVP and 0.01 wt% CMC.

substrate yet have different demands on the properties of the feed dispersion and yield different layer structures. The Langmuir deposition technique has good prospects of generating additive-free coatings from water-immiscible spreading solvents such as DCE, the spray coater is versatile and handles different dispersions well, while direct ink-jet printing could be used for the preparation of structured layers. The often-reported vacuum filtration is known to yield conductive and compact films. However, this technique cannot be performed on non-porous substrates and the compact graphene layers are inaccessible to reactants. Consequently, this technique cannot be applied for some of the possible applications.

With the high inherent conductivity of the individual few-layer gpG flakes, the main source of resistance in a layer is the interface resistance between the particles. However, high porosity and roughness are beneficial for interface-driven chemical processes in liquid and gas phase. Therefore, conductivity and accessibility of the surface by porosity and roughness are key thin film properties which need to be balanced carefully in a compromise. Both are highly dependent on the layer formation and therefore on the graphene dispersion used. The proper choice of liquids and additives for a dispersion in this technical context depends on several factors.

- sedimentation stability of the dispersion
- evaporation and drying behavior
- surface energy and wetting of the substrate

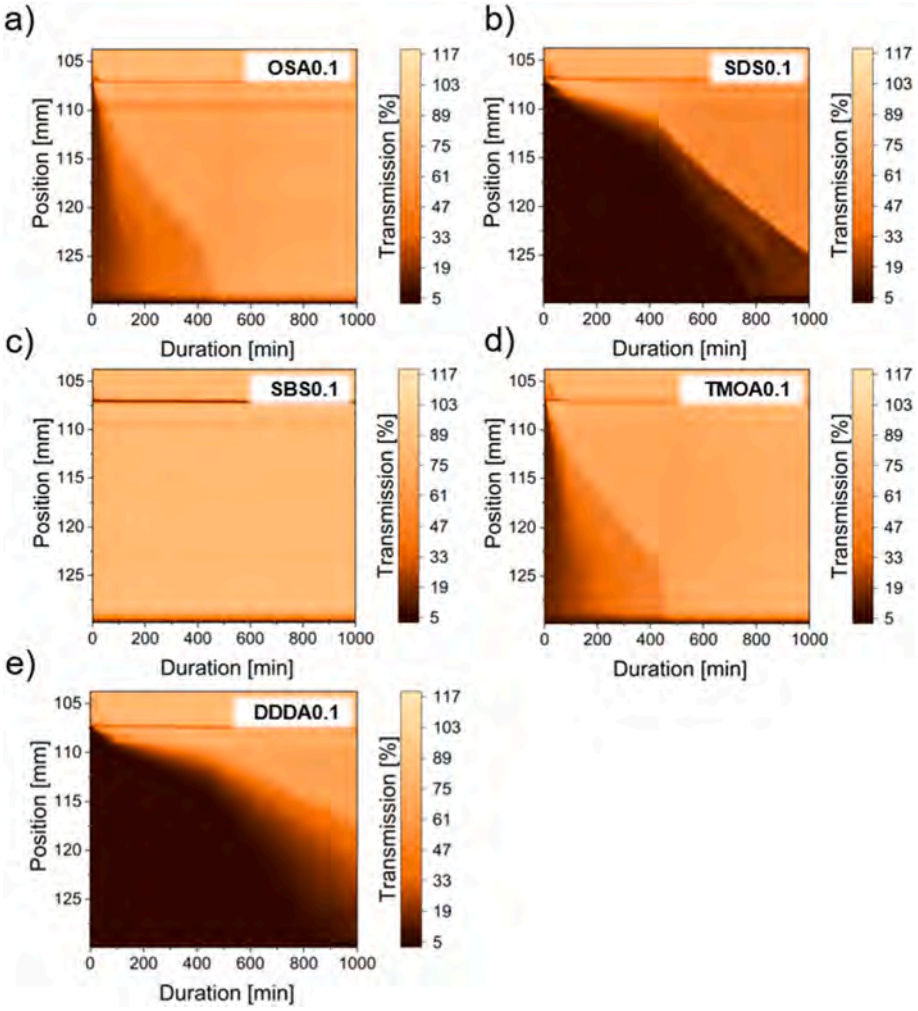

Fig. 6. Transmittograms for 0.1 wt% gpG in water with different surfactants as additives centrifuged with a relative acceleration of about 575 g. a) Water with 0.1 wt % sodium octyl sulfonate; b) with 0.1 wt% sodium dodecyl sulfate; c) with 0.1 wt% sodium benzoyl sulfonate; d) with 0.1 wt% trimethyloctylammonium bromide; e) with 0.1 wt% n-didodecyldimethylammonium bromide.

- in case of non-volatile additives: their compatibility with the desired application
- compatibility of possible additives with the materials of the coating device
- toxicity and environmental sustainability of the applied chemicals

3.4.2. *Transport characteristics of gpG thin films*

The carrier transport properties of the prepared layers on polished c-plane sapphire were characterized with results presented in Table 2. Transport measurements of a representative sample (Langmuir, 3x Layers) are presented in Figure S 9 and reveal linear current-voltage behavior characteristic of ohmic contacts and symmetric Hall responses under magnetic field reversal, demonstrating stable and reproducible charge transport. The individual measurements have a maximum relative error of about 1 %. To accurately determine the bulk three-dimensional conductivity, the thickness of the film is needed. However, the coatings are rough and uneven as will be discussed in detail later. Here the effective two-dimensional sheet resistivities and conductivities are therefore reported in Table 2. Furthermore, even an average thickness cannot represent the electron pathways properly since the main source of resistance is most likely due to points of limited contact of flakes both in lateral dimension as well as cross-sectional.

Four-point probe resistance, resistivity, and conductivity in a van der Pauw geometry were measured for spray-coated and Langmuir samples at varying numbers of layers by subsequent deposition. The printed

Table 2
As measured conductivity and transport properties of the prepared gpG thin films on polished sapphire.

Sample	Resistance	Sheet resistivity	Sheet conductivity	Hall mobility	Carrier density
	[kΩ]	[kΩ/sq]	[mS/sq]	[cm^2/V•s]	10^{14} [cm^{-2}]
Langmuir films					
1x Layer	17.76	80.46	0.01	4	0.2
2x Layer	1.59	7.20	0.14	11	0.8
3x Layer	1.12	5.43	0.18	19	0.6
Spray coating					
DDDA 15 passes	1.03	4.64	0.21	2	6.6
DDDA 25 passes	0.16	0.73	1.36	9	9.7
DDDA 35 passes	0.13	0.60	1.67	2	50.0
CMC 0.1 wt% 15 passes	0.18	0.83	1.20	9	8.9
CMC 0.1 wt% 25 passes	0.09	0.40	2.52	11	14.0
CMC 0.1 wt% 35 passes	0.12	0.52	1.92	6	20.0
	[kΩ]		[mS]		
Printing	0.23	-	4.3	-	-

samples have been measured using prepared Au/Cr electrodes on the substrates. The results for spray coated gpG films show clear trends: As expected, an increasing number of passes of the spray head increases the sheet conductivity for both CMC and DDDA. With the surfactant DDDA, conductivity rises to 1.67 mS/sq at 35 passes. The Hall mobility is in the range between 1 and 10 $cm^2/V•s$, while the sheet carrier density increases with thickness from $6.6•10^{14}$ to $9.7•10^{14}$ and finally to $50•10^{14}$ cm^{-2}. The mobilities are somewhat lower than the best values reported in the literature for printed graphene layers [95–97] and several orders of magnitude below the mobility of a single, suspended mechanically

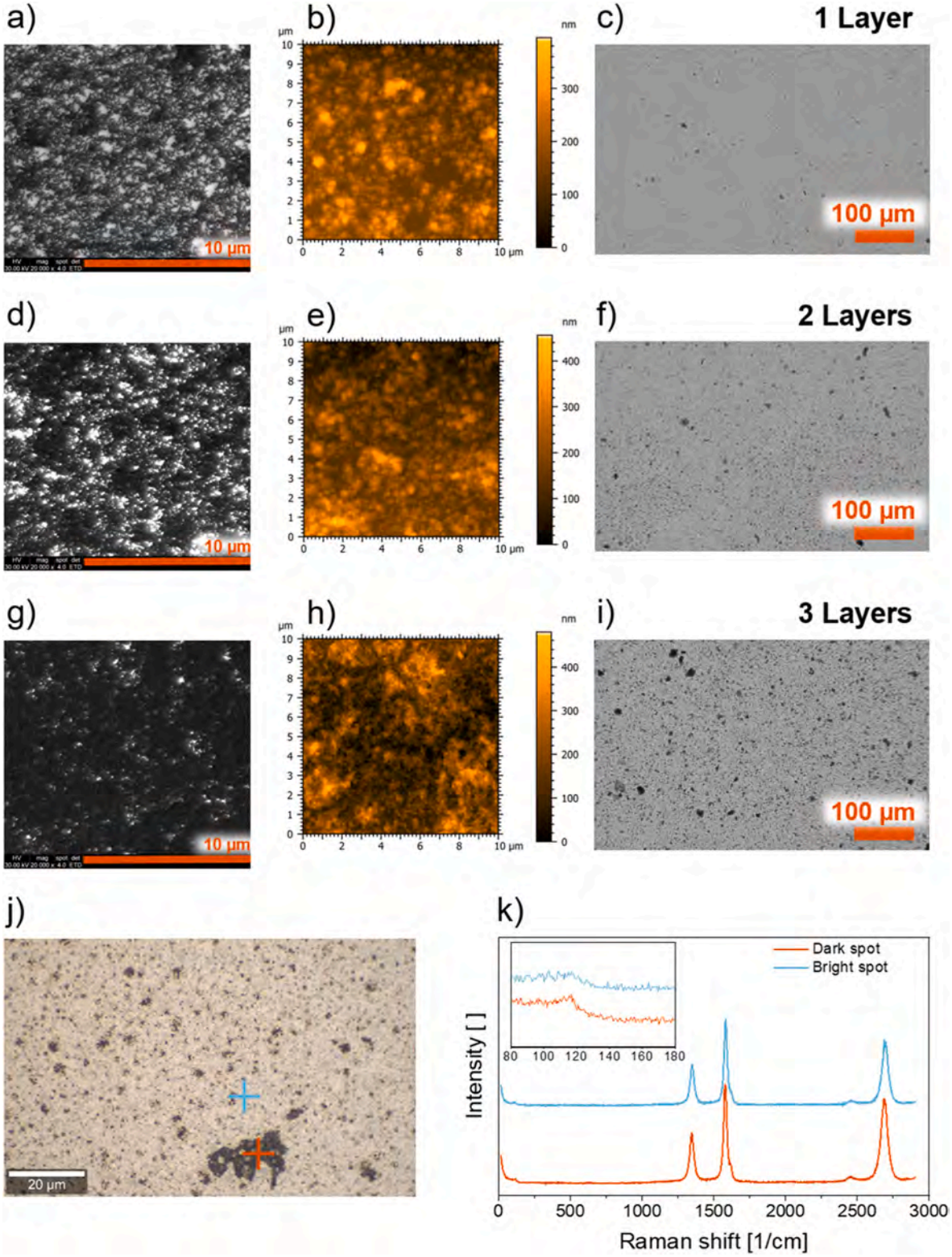

Fig. 7. Graphene thin films on sapphire prepared by Langmuir deposition characterized by SEM (left column), AFM (middle), transmission optical microscopy (right) and Raman spectroscopy (bottom). a-c) One deposition; d-f) two depositions; g-i) three subsequent depositions on the same substrate; j) and k) Raman spectroscopy of two distinctly different spots by one layer deposition, graphene layer breathing modes are in the marked region.

exfoliated graphene flake [98]. This shows that to form conductive layers of graphene, the flake-to-flake contact has a strong impact. In Fig. 1a, the wrinkled nature of gpG is apparent. This self-folding property of graphene from gas phase synthesis together with a complex interrelationship of liquids and additives opens many different options to tailor the coating properties, but also complicates interpretation. To better understand the film formation, microscopic imaging methods were applied and discussed for each coating technique in the following chapters.

3.4.3. Layer formation by Langmuir deposition

A first scalable method is the Langmuir deposition which yields additive-free graphene layers. The thin films prepared by this method are characterized by SEM, AFM, optical microscopy, and Raman spectroscopy. The results are presented in Fig. 7. The micrographs a-c) show the deposition of only one layer on the flat and insulating substrate. Gaps between the individual agglomerates remain, which are the main source of electrical resistance for these layers. This first kind of defects for this layer deposition method can be cured by simply adding more layers on top. As can be seen in the other micrographs for the two (d-f) or three (g-i) consecutive depositions, the gaps between the agglomerates are filled up and thus this kind of defect is cured which leads to the improved conductivity (Table 2). Layers of liquid-phase exfoliated flG [35] flakes did agglomerate much less on the surface of water, so that continuous coverage was possible with much less deposition. Furthermore, the conductivity increases linearly above a minimal threshold, whereas this threshold seems to be much higher in the case of gpG. This is due to the amplified agglomeration. Exemplary Raman spectra (Fig. 7j and k) were recorded to investigate this agglomeration of gpG combined with mappings of the 2D- and G-mode, presented in Figure S 10.

The low-frequency Raman mode at about 115 cm^{-1} is related to layer breathing modes of graphene plates, which are of low but identifiable magnitude. Furthermore, the FWHM values of the 2D signals of different Raman spectra from samples with one to three consecutive depositions with both bright and dark spots are compared, and no significant difference can be found. The values are in the range of 49.1 to 55.6 cm^{-1} and presented in Table S 4. This is also apparent by the mappings in Figure S 10. The only difference found is a higher intensity of the Raman signal for the dark spots compared to the bright spots, which is explained by the larger amount of material in those spots. For the agglomeration of graphene, many different geometries are imaginable, e.g.: plane-on-plane, edge-to-plane, corner-to-plane. However, the low intensity of the layer breathing mode, together with the characteristic 2D and G Raman features — both highly sensitive to layer number — suggests that extended plane-on-plane stacking is limited in the resulting films. Instead, the agglomeration and film assembly are likely governed by edge and corner interactions between the wrinkled gpG flakes, both laterally and vertically. This interpretation is consistent with SEM and AFM observations showing locally disordered, non-planar morphology. Further aspects on agglomeration are discussed in more details in the SI. In summary, the lack of three-dimensional movement in the surface film on water seems to limit the agglomeration to wrinkled structures instead of plane-on-plane agglomeration, even though it would reduce more the surface energy of the gpG flakes.

Another kind of defect occurs during the deposition. The graphene agglomerates on the surface of water seem to form a cohesive but brittle layer. As the water level is lowered at the end of the deposition, the graphene layer shrinks to adapt to the new geometry yet breaks under the tension. Consequently, gaps can be found in the layer. Furthermore, other gaps can be introduced by drying the layers. Examples of these kinds of defects are displayed in Figure S 11. While these gaps are apparent in the film with only one deposition, the addition of more layers on top also cures this defect. The lesser absorption of light of a gap in three layers of deposition is still visible in optical microscopy, yet the surface coverage is complete as seen in the AFM to the degree that the original gap is almost no longer detectable. The removal of these two kinds of defects is reflected in the improved conductivity as well, as seen in Table 2.

The influence of the dispersion on the layer formation is indirect for this method since the layer is initially formed on the surface of water. However, stability can be assumed as a necessity for the dispersion. If the dispersion is unstable (for instance in HEX), graphene would agglomerate fast in the syringe and tubes. Therefore, it cannot be cast carefully onto the surface of water and form a floating film. But this method does impose other demands onto the liquids used for the dispersions as it needs to spread and float on the water surface and needs to be immiscible in large parts with water to prevent mixing in the bulk. These demands have for gpG only been fulfilled by DCE simultaneously. Therefore, it remains the only possible option for the Langmuir deposition despite its unfavorable safety properties.

Considering these results in light of the Hall data, the following picture evolves. The Langmuir films exhibit much higher resistivity than spray coated films when only one layer is deposited (80 kΩ/sq) due to the gaps in the film. However, further addition of layers in the Langmuir films drastically lowers resistivity and raises conductivity (0.01 mS/sq for one layer to 0.18 mS/sq for three layers). The Hall mobility increases from 4 to 19 $cm^2/V\bullet s$, the highest among all three methods. This can be explained in a way that single layer Langmuir depositions leave gaps between agglomerated flakes on the substrate, which are the major source of resistance. Successive depositions fill these gaps, increasing flake-to-flake contacts and enhancing both conductivity and mobility.

3.4.4. Layer formation by ultrasonic spray coating

Ultrasonic spray coating is a well-known method to deposit thin films on flexible and rigid substrates from dispersions with different formulations. To investigate the relation of conductivity and the microstructure of the graphene layers produced by this method, the set of samples coated with gpG dispersed in water with DDDA are characterized by SEM, AFM and optical microscopy as displayed in Fig. 8. At this point it should be mentioned that the demands on dispersions mentioned above (stability, evaporation behavior, wetting, compatibility of additives) for a coating application have been considered for the selection of liquids and additives. The ultrasonic spray coater uses tubes and a syringe pump to control the flow of liquids to the nozzle. Critical components (common polymers such as Teflon, polyolefins) are compatible with water and alcohols, for limited contact time also with aprotic polar solvents like NMP or HEP.

In general, the layers appear to be rough and porous, with the coverage of the substrate increasing with each pass of the spray head. The roughness magnitude nearly exceeds the measurable range of the AFM. Nonetheless, the AFM micrographs show the flakes forming a thin film by agglomeration, yet the gpG flakes are not in compact arrangement just like the layers from the Langmuir deposition. The S_q roughness parameter (ISO 25178) from 15 to 35 layers is 340, 410 and 220 nm respectively as determined from the AFM micrographs. From the SEM and optical micrographs, it is apparent that the porosity is not reduced but maintained between subsequent passes of the spray nozzle, even forming foam-like cavities (Fig. 8i). These cavities are about 0.1 to 10 μm wide and internally rough due to the graphene folding, which is promising for heterogenous surface-limited processes, like catalysis and adsorption. Residues of DDDA bromide salt were not found in the micrographs. The electron transport properties therefore seem to be linked to the porous foam-like microstructure observed in the films that persist after successive passes. Such porosity limits flake-to-flake transport.

The thin films formed with other dispersion formulation (aqueous 0.1 and 1 wt% CMC, as well as organic HEP and EtOH) are described in detail in the SI (Figure S 12 – Figure S 16). In summary, the formulation with 0.1 wt% CMC is able to form a conductive layer with long-stretched island-like structures in between areas of less material. The features are of about 10 to 100 μm. The formulation with 1 wt% CMC however does form a cohesive polymer matrix, in which the gpG flakes are embedded. The thin film is not conductive. The two dispersions with organic liquids

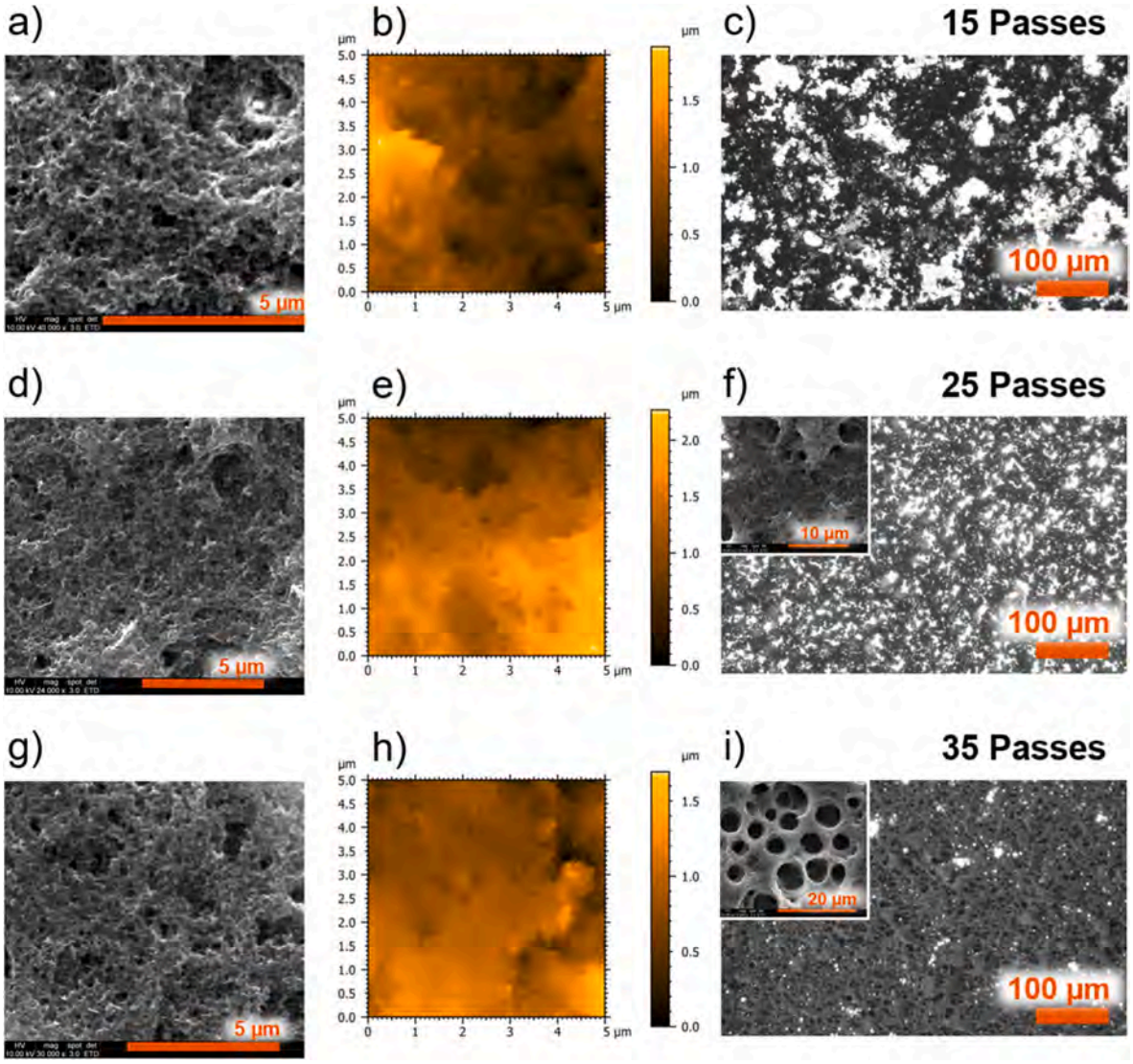

Fig. 8. Graphene thin films spray coated on sapphire from aqueous dispersion of gpG with DDDA cationic surfactant. Left: SEM micrographs, middle: AFM micrographs, right: transmission optical micrographs. a-c) 15 Passes of the ultrasound spray head, d-f) 25 passes, g-i) 35 passes. f and i) inset: SEM micrograph zooming into the porous microstructure, b) and h) note the distortions in parts with large slopes as the limitation of the AFM capabilities.

did not successfully yield thin films for scalable applications. HEP suffers from a low vapor pressure, which leads to ineffective drying and EtOH leads to unreliable results due to the lack of sedimentation stability.

Taken together, the results show that the formation of thin films prepared by the ultrasonic spray coater directly depends on the dispersion properties. The aqueous dispersions with additives show promising behavior. The stability is sufficient in the case of DDDA and CMC, as well as the evaporation fast enough for the fabrication. For these two cases, the additive shows a strong impact on the layer formation. As the surface energy seems to be lowered with DDDA and thus gas-bubbles stabilized, the gpG arranges in a foam-like manner forming a porous layer. For CMC, it is apparent that the additive can impact the layer formation negatively for the desired application with 1 wt%, while 0.1 wt% is compatible with a conductive thin film. However, the thin films with additives demonstrate the need for detailed optimization of these layers in terms of concentration and drying conditions like the length of the timeframe between each layer. In any case, the additives dominate the layer formation and thus the form and properties of the thin film. In contrast, EtOH does not fulfil the demands on stability against agglomeration. Therefore, the coverage is very unreliable, which is unsuited for scalable production. HEP on the other hand satisfies the demands on stability exceptionally well. However, the drying properties are not sufficient for the formation of coatings. Even at 150 °C, which is too high for most flexible substrates already, the evaporation is too slow for any practical purpose.

3.4.5. *Layers by ink-jet printing*

Finally, a third way to produce graphene layers is the use of ink-jet printing, which has been demonstrated with promising results with exfoliated graphene on flexible and rigid substrates in the past [37–39, 99]. Two different formulations were tested: one aqueous dispersion with 0.1 wt% gpG and 0.1 wt% PVP in water, as used similarly in other studies before (e.g. Ref. [39]), and one of 0.1 wt% gpG in DCB. The waterborne formulation led to immediate clogging of the printer's nozzles. This could also not be cured by further diluting the ink to only 0.025 wt% PVP and gpG. The organic ink with DCB was directly printable. While both dispersions were stable against sedimentation, the conformation of the particle (crumpled or flat) is unknown but can be decisive if the nozzle diameter is in the range of 10 to 100 times the particle diameter of some hundred nanometers (Fig. 1a).

Electrodes (Au on Cr) where prepared by lithography on a silicon thermal oxide wafer with a gap of 10 µm, and the gpG ink was printed

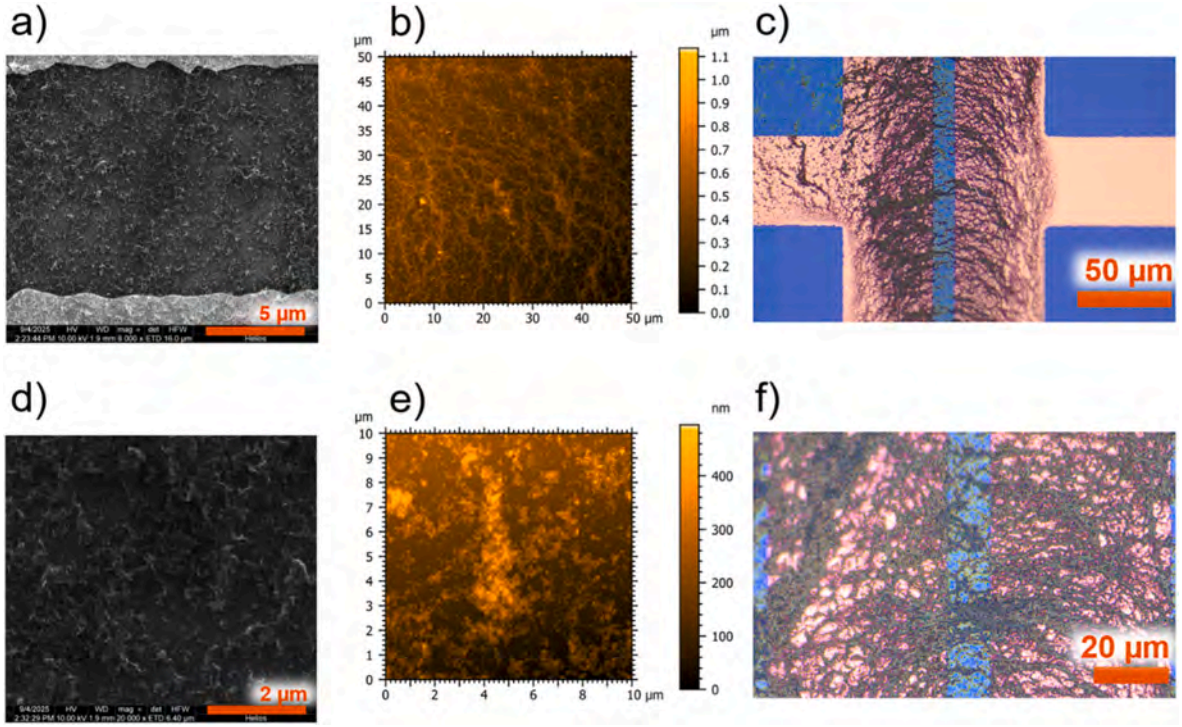

Fig. 9. Graphene ink jet printed from 1,2-dichlorobenzene dispersion on electrodes, characterized by SEM (a and d), AFM (b and e) and optical microscopy (c and f).

between the two electrodes. The characterization of the gpG by SEM, AFM and optical microscopy is presented in Fig. 9.

These micrographs show that gpG agglomerates during the drying of the layer forming web-like structures stretching from one electrode to the other. In between some individual isolated agglomerates are apparent in the AFM micrographs. This first printing with the new material gpG already provides some conductivity of 4.3 mS. Similar web-like layer formation has been found for liquid phase exfoliated modified graphene by Arapov et al. on porous substrates [38]. Depending on the substrate and the modification of the graphene, the coverage could be improved. On rigid Si substrates, Torrisi et al. found a strong dependency of the coverage with the surface preparation, hydrophobic surfaces showed the best results. This indicates that like for the spray-coated samples with CMC, the drying step can be optimized to reliably provide high-quality graphene thin films. To improve the surface coverage and thus the conductivity and precision of the printing, surface preparation should be considered, which might improve the wetting of the substrate by the hydrophobic DCB. Furthermore, to enhance the drying limited by the device to a maximum temperature of 50 °C, DCB might be exchanged with DCE, which provides similar stability and wetting properties, but evaporates much faster. However, the results show that gpG can be printed as an ink with DCB just like exfoliated flG which is as seen for the aqueous dispersion not guaranteed. The detailed optimization, however, is subject to future research beyond the scope of this work.

4. Conclusion

In this work, the applicability of gas-phase synthesized graphene (gpG) for the fabrication of thin films is investigated by a systematic approach to formulate and evaluate stable dispersions and conductive thin films. Using space- and time-resolved analytical centrifugation (AC), the dispersion stability was quantitatively assessed in-situ. AC as a method with accelerated sedimentation allows for the fast screening of several dispersion formulations and subsequent improvement of the formulation as well as the differentiation of different sedimentation modes – without the need for a mathematical sedimentation model. The results identify flake agglomeration, intensified by the anisotropic geometry of gpG, as the main cause of destabilization.

From the results of AC, Hansen parameters (HSPs) were calculated for stable gpG dispersions: $\delta_D = 17.81$ MPa$^{1/2}$, $\delta_P = 12.84$ MPa$^{1/2}$ and $\delta_H = 9.1$ MPa$^{1/2}$. In comparison to previously published results, the polar interaction is emphasized with a larger value. However, in the past, results were achieved by evaluating the concentration and stability of exfoliated graphene. Therefore, they included the stabilization as well as the exfoliation, whereas the HSPs in this study represent the stabilization alone. Furthermore, it should be considered that the exfoliation also depends on kinetic factors such as diffusion and thus the particle size.

The HSPs for stable dispersions in this study appear to be very narrow. While NMP yields a suspension with immeasurable slow sedimentation, DMF is only stable for 10 min of centrifugation. Furthermore, if other liquids which yield stable dispersions outside of the HSP study of this work are considered (HEP, DCE, DCB), the HSPs becomes less clear, as stable dispersions can be found further away from the calculated value. Thus, the stability of a dispersion with gpG does not seem to be predictable by HSPs alone. Another interpretation is the formation of energy barriers between the graphene flakes. These require proper solvent–particle or solvent–additive–particle interactions. For a probe liquid to stabilize the dispersion, its molecular structure should have *amphiphilic* properties: one side of the molecule should be attractive by a strong dipole which can orient towards the graphene plane, the other should be less attractive with apolar hydrocarbon bonds, consequently creating an energy barrier between the two graphene flakes. Additives seem to stabilize the gpG dispersions by both DLVO and non-DLVO mechanisms. Hence, stability is not a matter of thermodynamics alone, but depends on kinetic phenomena.

This way, stable dispersions were achieved both in pure organic liquids and in aqueous systems with green non-toxic additives. Among pure liquids, γ-lactam compounds, NMP and HEP as well as the chlorinated liquids DCB, and DCE produced the most stable dispersions, confirming that well-dispersed gpG can be obtained without oxidation or chemical modification. In water, the polymers CMC, PVP, and the cationic surfactant DDDA enabled stable formulations using only mild sonication for 5 min, offering environmentally benign alternatives to

organic media.

For a successful formation of a thin film, a dispersion of gpG has to meet requirements with respect to the coating technique. Langmuir deposition requires a dispersion stable within the timeframe of the process, furthermore, the liquid needs to have a much lower surface tension to spread on the water surface and finally evaporate quickly under ambient conditions. This has, so far, only been fulfilled by DCE simultaneously. Although requiring multiple layers for complete coverage, the method allowed to produce additive-free films with the highest carrier mobility (≈19 $cm^2/V\bullet s$), preserving the intrinsic transport of gpG flakes. Improvements for this method might be of geometric nature in order to minimize the formation of cracks.

For ultrasonic spray coatings, the dispersion must be stable as well, the drying should be possible at reasonable temperatures without damaging the substrate, and possible additives should not be incompatible with the desired application. With DDDA and CMC, two additives have been found which fulfil these requirements. The layers formed by 0.1 wt% CMC are rough yet compact (conductivity ≈ 2.5 mS/sq, mobility ≈ 11 $cm^2/V\bullet s$), while the layers by DDDA have a rough, foam-like structure and exhibited lower mobility. However, if the content of CMC in the dispersion is too high, the layer becomes insulating as the flakes are isolated in the polymer matrix. It is therefore apparent that the formation of thin films by ultrasonic spray coating is a matter of further detailed optimization regarding the type and concentration of additives and the drying condition (temperature and time between each layer). Furthermore, due to the strong impact of additives such as surfactants and polymers, future work on the thin film formation of gpG related materials should focus on the particle-additive interaction during the film formation. It is possible that the transport properties can be improved further by post-treatment methods which focus on the modification or even removal of such additives.

Finally, inkjet printing proved feasible for organic dispersions but still faces challenges with drying and nozzle clogging for aqueous dispersions. However, before an optimization of the process can be pursued, the conditions under which a droplet of ink can be formed reliably without clogging the nozzles should be studied. It is likely that the particle form, determined by its chemical environment, is a vital factor which needs to be controlled. Once this is understood and controlled by the ink formulation, the drying conditions and possibly surface preparation can be adjusted to optimize the thin-film formation. By this, inkjet printing of gpG might add a valuable method for the fabrication of flexible electronics under ambient low-temperature conditions.

Overall, the study establishes clear processing-structure-property-relationships for gpG systems: dispersion stability and drying behavior dictates film uniformity, which in turn governs charge transport. While each of the individual methods for characterization as well as for thin-film formation are not novel on its own, their combination in this study facilitates the technical integration of this new and promising material gpG. The findings provide a foundation of empirical and mechanistic knowledge for scalable, additive-controlled, or additive-free coating strategies and highlight gpG's potential beyond lithium-ion batteries, particularly in electronic, catalytic, and sensing applications. Future work can use this study as a steppingstone for application of gas-phase synthesized graphene-related materials in applications.

CRediT authorship contribution statement

Lars Grebener: Writing – review & editing, Writing – original draft, Visualization, Methodology, Investigation, Data curation, Conceptualization. **Yasaman Jarrahizadeh:** Writing – review & editing, Writing – original draft, Validation, Methodology, Investigation, Data curation. **Shaghayegh Pourdahrany:** Writing – original draft, Investigation. **Muhammad Ali:** Investigation. **Nicholas D. Wilson:** Methodology, Investigation. **Oliver Altenhoff:** Investigation, Formal analysis, Data curation. **Stuart Goldie:** Writing – review & editing, Methodology. **Marika Schleberger:** Writing – review & editing, Supervision, Project administration. **Axel Lorke:** Writing – review & editing, Supervision, Project administration. **William Wong:** Writing – review & editing, Supervision, Project administration. **Hartmut Wiggers:** Writing – review & editing, Supervision, Project administration. **Michael A. Pope:** Writing – review & editing, Supervision, Project administration. **Mohaned Hammad:** Writing – review & editing, Writing – original draft, Supervision, Project administration, Conceptualization. **Doris Segets:** Writing – review & editing, Writing – original draft, Supervision, Project administration, Conceptualization.

Declaration of competing interest

The authors declare that they have no known competing financial interests or personal relationships that could have appeared to influence the work reported in this paper.

Acknowledgement

Financial support of this work by the Deutsche Forschungsgemeinschaft (DFG, German Research Foundation) project number 461605777 (IRTG 2803 2D MATURE) and of the Natural Sciences and Engineering Council of Canada (NSERC, CREATE 565360) is gratefully acknowledged. The authors would also like to thank the Interdisciplinary Center for Analytics on the Nanoscale (ICAN) for the support of this work with substantial analytical measurements.

Appendix A. Supplementary data

Supplementary data to this article can be found online at https://doi.org/10.1016/j.carbon.2026.121365.

Data availability

Data is available on Nomad-Lab. DOI: 10.17172/NOMAD/2026.02.12-2

References

[1] K.S. Novoselov, A.K. Geim, S.V. Morozov, D. Jiang, Y. Zhang, S.V. Dubonos, I. V. Grigorieva, A.A. Firsov, Science (New York, N.Y.) 306 (5696) (2004) 666–669, https://doi.org/10.1126/science.1102896.
[2] T.S. Tran, N.K. Dutta, N.R. Choudhury, Adv. Colloid Interface Sci. 261 (2018) 41–61, https://doi.org/10.1016/j.cis.2018.09.003.
[3] D.W. Johnson, B.P. Dobson, K.S. Coleman, Curr. Opin. Colloid Interface Sci. 20 (5-6) (2015) 367–382, https://doi.org/10.1016/j.cocis.2015.11.004.
[4] J. Texter, Curr. Opin. Colloid Interface Sci. 19 (2) (2014) 163–174, https://doi.org/10.1016/j.cocis.2014.04.004.
[5] S. Park, R.S. Ruoff, Nat. Nanotechnol. 4 (4) (2009) 217–224, https://doi.org/10.1038/nnano.2009.58.
[6] M.M. Gudarzi, M.H.M. Moghadam, F. Sharif, Carbon 64 (2013) 403–415, https://doi.org/10.1016/j.carbon.2013.07.093.
[7] A. Lerf, Solid State Ionics 101–103 (1997) 857–862, https://doi.org/10.1016/S0167-2738(97)00319-6.
[8] C. Hontoria-Lucas, A.J. López-Peinado, J.D. López-González, M.L. Rojas-Cervantes, R.M. Martín-Aranda, Carbon 33 (11) (1995) 1585–1592, https://doi.org/10.1016/0008-6223(95)00120-3.
[9] I. Ogino, Y. Yokoyama, S. Iwamura, S.R. Mukai, Chem. Mater. 26 (10) (2014) 3334–3339, https://doi.org/10.1021/cm501305c.
[10] Q. Zheng, L. Shi, P.-C. Ma, Q. Xue, J. Li, Z. Tang, J. Yang, RSC Adv. 3 (14) (2013) 4680, https://doi.org/10.1039/C3RA22367A.
[11] M. Wojtoniszak, X. Chen, R.J. Kalenczuk, A. Wajda, J. Łapczuk, M. Kurzewski, M. Drozdzik, P.K. Chu, E. Borowiak-Palen, Colloids and surfaces. B, Biointerfaces 89 (2012) 79–85, https://doi.org/10.1016/j.colsurfb.2011.08.026.
[12] M. Fang, J. Long, W. Zhao, L. Wang, G. Chen, Langmuir : the ACS journal of surfaces and colloids 26 (22) (2010) 16771–16774, https://doi.org/10.1021/la102703b.
[13] W. Zhao, F. Wu, H. Wu, G. Chen, J. Nanomater. (1) (2010), https://doi.org/10.1155/2010/528235, 2010.
[14] Y. Liang, D. Wu, X. Feng, K. Müllen, Adv. Mater. 21 (17) (2009) 1679–1683, https://doi.org/10.1002/adma.200803160.
[15] F. Li, Y. Bao, J. Chai, Q. Zhang, D. Han, L. Niu, Langmuir : the ACS journal of surfaces and colloids 26 (14) (2010) 12314–12320, https://doi.org/10.1021/la101534n.

[16] D. Konios, M.M. Stylianakis, E. Stratakis, E. Kymakis, J. Colloid Interface Sci. 430 (2014) 108–112, https://doi.org/10.1016/j.jcis.2014.05.033.
[17] C. Zhang, W.W. Tjiu, W. Fan, S. Huang, T. Liu, J. Mater. Chem. 22 (23) (2012) 11748, https://doi.org/10.1039/C2JM30955F.
[18] F.J. Tölle, M. Fabritius, R. Mülhaupt, Adv Funct Materials 22 (6) (2012) 1136–1144, https://doi.org/10.1002/adfm.201102888.
[19] S. Pei, H.-M. Cheng, Carbon 50 (9) (2012) 3210–3228, https://doi.org/10.1016/j.carbon.2011.11.010.
[20] H.C. Schniepp, J.-L. Li, M.J. McAllister, H. Sai, M. Herrera-Alonso, D.H. Adamson, R.K. Prud'homme, R. Car, D.A. Saville, I.A. Aksay, J. Phys. Chem. B 110 (17) (2006) 8535–8539, https://doi.org/10.1021/jp060936f.
[21] J.I. Paredes, S. Villar-Rodil, P. Solís-Fernández, A. Martínez-Alonso, J.M.D. Tascón, Langmuir : the ACS journal of surfaces and colloids 25 (10) (2009) 5957–5968, https://doi.org/10.1021/la804216z.
[22] D. Zhou, Q.-Y. Cheng, B.-H. Han, Carbon 49 (12) (2011) 3920–3927, https://doi.org/10.1016/j.carbon.2011.05.030.
[23] D. Li, M.B. Müller, S. Gilje, R.B. Kaner, G.G. Wallace, Nat. Nanotechnol. 3 (2) (2008) 101–105, https://doi.org/10.1038/nnano.2007.451.
[24] W. Zhang, W. He, X. Jing, J. Phys. Chem. B 114 (32) (2010) 10368–10373, https://doi.org/10.1021/jp1037443.
[25] A. Münzer, L. Xiao, Y.H. Sehlleier, C. Schulz, H. Wiggers, Electrochim. Acta 272 (2018) 52–59, https://doi.org/10.1016/j.electacta.2018.03.137.
[26] S. Ahadian, M. Estili, V.J. Surya, J. Ramón-Azcón, X. Liang, H. Shiku, M. Ramalingam, T. Matsue, Y. Sakka, H. Bae, K. Nakajima, Y. Kawazoe, A. Khademhosseini, Nanoscale 7 (15) (2015) 6436–6443, https://doi.org/10.1039/C4NR07569B.
[27] S. De, P.J. King, M. Lotya, A. O'Neill, E.M. Doherty, Y. Hernandez, G.S. Duesberg, J. N. Coleman, Small 6 (3) (2010) 458–464, https://doi.org/10.1002/smll.200901162.
[28] J. Luo, L. Yang, D. Sun, Z. Gao, K. Jiao, J. Zhang, Small 16 (45) (2020) e2003426, https://doi.org/10.1002/smll.202003426.
[29] K. Arapov, E. Rubingh, R. Abbel, J. Laven, G. de With, H. Friedrich, Adv Funct Materials 26 (4) (2016) 586–593, https://doi.org/10.1002/adfm.201504030.
[30] P. He, J. Sun, S. Tian, S. Yang, S. Ding, G. Ding, X. Xie, M. Jiang, Chem. Mater. 27 (1) (2015) 218–226, https://doi.org/10.1021/cm503782p.
[31] Z. Sun, J. Masa, Z. Liu, W. Schuhmann, M. Muhler, Chemistry (Weinheim an der Bergstrasse, Germany) 18 (22) (2012) 6972–6978, https://doi.org/10.1002/chem.201103253.
[32] Z. Khanam, J. Liu, S. Song, J Nanopart Res 23 (8) (2021), https://doi.org/10.1007/s11051-021-05294-2.
[33] A. Al Shboul, C. Trudeau, S. Cloutier, M. Siaj, J.P. Claverie, Nanoscale 9 (28) (2017) 9893–9901, https://doi.org/10.1039/C7NR01919J.
[34] E. Bertin, A. Münzer, S. Reichenberger, R. Streubel, T. Vinnay, H. Wiggers, C. Schulz, S. Barcikowski, G. Marzun, Appl. Surf. Sci. 467–468 (2019) 1181–1186, https://doi.org/10.1016/j.apsusc.2018.10.061.
[35] H. Kim, C. Mattevi, H.J. Kim, A. Mittal, K.A. Mkhoyan, R.E. Riman, M. Chhowalla, Nanoscale 5 (24) (2013) 12365–12374, https://doi.org/10.1039/c3nr02907g.
[36] X. Li, G. Zhang, X. Bai, X. Sun, X. Wang, E. Wang, H. Dai, Nat. Nanotechnol. 3 (9) (2008) 538–542, https://doi.org/10.1038/nnano.2008.210.
[37] E.B. Secor, P.L. Prabhumirashi, K. Puntambekar, M.L. Geier, M.C. Hersam, J. Phys. Chem. Lett. 4 (8) (2013) 1347–1351, https://doi.org/10.1021/jz400644c.
[38] K. Arapov, R. Abbel, G. de With, H. Friedrich, Faraday Discuss. 173 (2014) 323–336, https://doi.org/10.1039/c4fd00067f.
[39] T. Juntunen, H. Jussila, M. Ruoho, S. Liu, G. Hu, T. Albrow-Owen, L.W.T. Ng, R.C. T. Howe, T. Hasan, Z. Sun, I. Tittonen, Adv Funct Materials 28 (22) (2018), https://doi.org/10.1002/adfm.201800480.
[40] N. Liu, F. Luo, H. Wu, Y. Liu, C. Zhang, J. Chen, Adv Funct Materials 18 (10) (2008) 1518–1525, https://doi.org/10.1002/adfm.200700797.
[41] U. Khan, H. Porwal, A. O'Neill, K. Nawaz, P. May, J.N. Coleman, Langmuir : the ACS journal of surfaces and colloids 27 (15) (2011) 9077–9082, https://doi.org/10.1021/la201797h.
[42] S. Ravula, S.N. Baker, G. Kamath, G.A. Baker, Nanoscale 7 (10) (2015) 4338–4353, https://doi.org/10.1039/C4NR01524J.
[43] Y. Arao, M. Kubouchi, Carbon 95 (2015) 802–808, https://doi.org/10.1016/j.carbon.2015.08.108.
[44] Y. Hernandez, V. Nicolosi, M. Lotya, F.M. Blighe, Z. Sun, S. De, I.T. McGovern, B. Holland, M. Byrne, Y.K. Gun'Ko, J.J. Boland, P. Niraj, G. Duesberg, S. Krishnamurthy, R. Goodhue, J. Hutchison, V. Scardaci, A.C. Ferrari, J. N. Coleman, Nat. Nanotechnol. 3 (9) (2008) 563–568, https://doi.org/10.1038/nnano.2008.215.
[45] A. O'Neill, U. Khan, P.N. Nirmalraj, J. Boland, J.N. Coleman, J. Phys. Chem. C 115 (13) (2011) 5422–5428, https://doi.org/10.1021/jp110942e.
[46] Y. Shin, X. Just-Baringo, M. Zarattini, L.H. Isherwood, A. Baidak, K. Kostarelos, I. Larrosa, C. Casiraghi, Mol. Syst. Des. Eng. 4 (3) (2019) 503–510, https://doi.org/10.1039/C9ME00024K.
[47] C.E. Hamilton, J.R. Lomeda, Z. Sun, J.M. Tour, A.R. Barron, Nano Lett. 9 (10) (2009) 3460–3462, https://doi.org/10.1021/nl9016623.
[48] J. Li, F. Ye, S. Vaziri, M. Muhammed, M.C. Lemme, M. Östling, Carbon 50 (8) (2012) 3113–3116, https://doi.org/10.1016/j.carbon.2012.03.011.
[49] U. Khan, A. O'Neill, M. Lotya, S. De, J.N. Coleman, Small 6 (7) (2010) 864–871, https://doi.org/10.1002/smll.200902066.
[50] J.N. Coleman, Accounts Chem. Res. 46 (1) (2013) 14–22, https://doi.org/10.1021/ar300009f.
[51] M. Lotya, Y. Hernandez, P.J. King, R.J. Smith, V. Nicolosi, L.S. Karlsson, F. M. Blighe, S. De, Z. Wang, I.T. McGovern, G.S. Duesberg, J.N. Coleman, J. Am. Chem. Soc. 131 (10) (2009) 3611–3620, https://doi.org/10.1021/ja807449u.
[52] M. Lotya, P.J. King, U. Khan, S. De, J.N. Coleman, ACS Nano 4 (6) (2010) 3155–3162, https://doi.org/10.1021/nn1005304.
[53] C. Knieke, A. Berger, M. Voigt, R.N.K. Taylor, J. Röhrl, W. Peukert, Carbon 48 (11) (2010) 3196–3204, https://doi.org/10.1016/j.carbon.2010.05.003.
[54] A.S. Buinov, E.R. Gafarova, E.A. Grebenik, K.N. Bardakova, B.C. Kholkhoev, N. N. Veryasova, P.V. Nikitin, N.V. Kosheleva, B.S. Shavkuta, A.S. Kuryanova, V. F. Burdukovskii, P.S. Timashev, Polymers 14 (18) (2022), https://doi.org/10.3390/polym14183792.
[55] S. Das, A.S. Wajid, J.L. Shelburne, Y.-C. Liao, M.J. Green, ACS Appl. Mater. Interfaces 3 (6) (2011) 1844–1851, https://doi.org/10.1021/am1011436.
[56] A.S. Wajid, S. Das, F. Irin, H.T. Ahmed, J.L. Shelburne, D. Parviz, R.J. Fullerton, A. F. Jankowski, R.C. Hedden, M.J. Green, Carbon 50 (2) (2012) 526–534, https://doi.org/10.1016/j.carbon.2011.09.008.
[57] L. Guardia, M.J. Fernández-Merino, J.I. Paredes, P. Solís-Fernández, S. Villar-Rodil, A. Martínez-Alonso, J. Tascón, Carbon 49 (5) (2011) 1653–1662, https://doi.org/10.1016/j.carbon.2010.12.049.
[58] R.J. Smith, M. Lotya, J.N. Coleman, New J. Phys. 12 (12) (2010) 125008, https://doi.org/10.1088/1367-2630/12/12/125008.
[59] F. Liu, C. Wang, X. Sui, M.A. Riaz, M. Xu, L. Wei, Y. Chen, Carbon Energy 1 (2) (2019) 173–199, https://doi.org/10.1002/cey2.14.
[60] M. Lotya, A. Rakovich, J.F. Donegan, J.N. Coleman, Nanotechnology 24 (26) (2013) 265703, https://doi.org/10.1088/0957-4484/24/26/265703.
[61] M. Ayán-Varela, J.I. Paredes, S. Villar-Rodil, R. Rozada, A. Martínez-Alonso, J. Tascón, Carbon 75 (2014) 390–400, https://doi.org/10.1016/j.carbon.2014.04.018.
[62] Y. Hernandez, M. Lotya, D. Rickard, S.D. Bergin, J.N. Coleman, Langmuir : the ACS journal of surfaces and colloids 26 (5) (2010) 3208–3213, https://doi.org/10.1021/la903188a.
[63] M. Yi, Z. Shen, X. Zhang, S. Ma, J. Phys. D Appl. Phys. 46 (2) (2013) 25301, https://doi.org/10.1088/0022-3727/46/2/025301.
[64] J. Walter, T.J. Nacken, C. Damm, T. Thajudeen, S. Eigler, W. Peukert, Small 11 (7) (2015) 814–825, https://doi.org/10.1002/smll.201401940.
[65] S. Goldie, S. Ott, A. Dawson, T. Starke, C. Gabbett, V. Vega-Mayoral, K. Synnatschke, M. Horn, J.N. Coleman, C. Backes, Adv Materials Inter 12 (24) (2025), https://doi.org/10.1002/admi.202500717.
[66] C.M. Sims, J.P. Killgore, E. Mansfield, J.R. Downing, A.C.M. de Moraes, M. C. Hersam, J.A. Fagan, Small 21 (20) (2025) e2410459, https://doi.org/10.1002/smll.202410459.
[67] T. Detloff, T. Sobisch, D. Lerche, Part & Part Syst Charact 23 (2) (2006) 184–187, https://doi.org/10.1002/ppsc.200601028.
[68] T. Sobisch, D. Lerche, Colloid Polym. Sci. 278 (4) (2000) 369–374, https://doi.org/10.1007/s003960050527.
[69] D. Lerche, T. Sobisch, J. Dispersion Sci. Technol. 32 (12) (2011) 1799–1811, https://doi.org/10.1080/01932691.2011.616365.
[70] A.S. Amin, A. Caidi, T. Lange, I. Radev, D.J.S. Sandbeck, W. Philippi, M.-A. Kräenbring, M. Öztürk, V. Peinecke, D. Lerche, F. Özcan, D. Segets, Part. Part. Syst. Char. 42 (1) (2025), https://doi.org/10.1002/ppsc.202400069.
[71] A.S. Amin, D. Lerche, A.S. Odungat, S.U. Boehm, T. Koch, F. Özcan, D. Segets, ChemCatChem 16 (6) (2024), https://doi.org/10.1002/cctc.202301393.
[72] M. Park, K. Song, T. Lee, J. Cha, I. Lyo, B.-S. Kim, ACS Appl. Mater. Interfaces 8 (33) (2016) 21595–21602, https://doi.org/10.1021/acsami.6b07272.
[73] T. Skaltsas, X. Ke, C. Bittencourt, N. Tagmatarchis, J. Phys. Chem. C 117 (44) (2013) 23272–23278, https://doi.org/10.1021/jp4057048.
[74] S. Süß, T. Sobisch, W. Peukert, D. Lerche, D. Segets, Adv. Powder Technol. 29 (7) (2018) 1550–1561, https://doi.org/10.1016/j.apt.2018.03.018.
[75] S. Bapat, D. Segets, ACS Appl. Nano Mater. 3 (8) (2020) 7384–7391, https://doi.org/10.1021/acsanm.0c01467.
[76] S. Bapat, S.O. Kilian, H. Wiggers, D. Segets, Nanoscale Adv. 3 (15) (2021) 4400–4410, https://doi.org/10.1039/D1NA00405K.
[77] S. Bapat, C. Giehl, S. Kohsakowski, V. Peinecke, M. Schäffler, D. Segets, Adv. Powder Technol. 32 (10) (2021) 3845–3859, https://doi.org/10.1016/j.apt.2021.08.030.
[78] O. Anwar, S. Bapat, J. Ahmed, X. Xie, J. Sun, D. Segets, Nanoscale 14 (37) (2022) 13593–13607, https://doi.org/10.1039/d2nr02711a.
[79] O. Anwar, A.S. Amin, A. Amin, M.-A. Kräenbring, F. Özcan, D. Segets, Part. Part. Syst. Char. 40 (11) (2023), https://doi.org/10.1002/ppsc.202300050.
[80] S. Süß, W. Lin, O. Getmanenko, L. Pflug, T. Sobisch, W. Peukert, D. Lerche, D. Segets, Particuology 44 (2019) 71–79, https://doi.org/10.1016/j.partic.2018.05.010.
[81] D. Lerche, T. Sobisch, Colloids Surf. A Physicochem. Eng. Asp. 440 (2014) 122–130, https://doi.org/10.1016/j.colsurfa.2012.10.015.
[82] S. Abbott, Curr. Opin. Colloid Interface Sci. 48 (2020) 65–76, https://doi.org/10.1016/j.cocis.2020.03.007.
[83] L. Xu, A.R. Tetreault, H.H. Khaligh, I.A. Goldthorpe, S.D. Wettig, M.A. Pope, Langmuir : the ACS journal of surfaces and colloids 35 (1) (2019) 51–59, https://doi.org/10.1021/acs.langmuir.8b03173.
[84] L.J. van der Pauw, Philips Res. Rep. (13) (1958) 1–9.
[85] C.-F. López-Cámara, P. Fortugno, M. Heidelmann, H. Wiggers, C. Schulz, Carbon 218 (2024) 118732, https://doi.org/10.1016/j.carbon.2023.118732.
[86] C.-J. Shih, S. Lin, M.S. Strano, D. Blankschtein, J. Am. Chem. Soc. 132 (41) (2010) 14638–14648, https://doi.org/10.1021/ja1064284.
[87] S. Lin, C.-J. Shih, M.S. Strano, D. Blankschtein, J. Am. Chem. Soc. 133 (32) (2011) 12810–12823, https://doi.org/10.1021/ja2048013.
[88] S.J. Goldie, M.T. Degiacomi, S. Jiang, S.J. Clark, V. Erastova, K.S. Coleman, ACS Nano 16 (10) (2022) 16109–16117, https://doi.org/10.1021/acsnano.2c04406.

[89] F. Müller, W. Peukert, R. Polke, F. Stenger, Int. J. Miner. Process. 74 (2004) S31–S41, https://doi.org/10.1016/j.minpro.2004.07.023.
[90] J. Luo, H.D. Jang, T. Sun, L. Xiao, Z. He, A.P. Katsoulidis, M.G. Kanatzidis, J. M. Gibson, J. Huang, ACS Nano 5 (11) (2011) 8943–8949.
[91] K. Holmberg, in: Ullmann's Encyclopedia of Industrial Chemistry, Wiley-VCH Verlag GmbH & Co. KGaA, Weinheim, Germany, 2000, p. 1.
[92] G. Gadelha, M.S. Nawaz, N.P. Hankins, S.J. Khan, R. Wang, C.Y. Tang, Desalination 354 (2014) 97–106, https://doi.org/10.1016/j.desal.2014.09.009.
[93] G. Para, A. Hamerska-Dudra, K.A. Wilk, P. Warszyński, Colloids Surf. A Physicochem. Eng. Asp. 365 (1-3) (2010) 215–221, https://doi.org/10.1016/j.colsurfa.2010.02.004.
[94] M.J. Fernández-Merino, J.I. Paredes, S. Villar-Rodil, L. Guardia, P. Solís-Fernández, D. Salinas-Torres, D. Cazorla-Amorós, E. Morallón, A. Martínez-Alonso, J. Tascón, Carbon 50 (9) (2012) 3184–3194, https://doi.org/10.1016/j.carbon.2011.10.039.
[95] G. Calabrese, L. Pimpolari, S. Conti, F. Mavier, S. Majee, R. Worsley, Z. Wang, F. Pieri, G. Basso, G. Pennelli, K. Parvez, D. Brooks, M. Macucci, G. Iannaccone, K. S. Novoselov, C. Casiraghi, G. Fiori, Nanoscale 12 (12) (2020) 6708–6716, https://doi.org/10.1039/C9NR09289G.
[96] Y. Wang, Y. Chen, S.D. Lacey, L. Xu, H. Xie, T. Li, V.A. Danner, L. Hu, Mater. Today 21 (2) (2018) 186–192, https://doi.org/10.1016/j.mattod.2017.10.008.
[97] K.S. Vasu, B. Chakraborty, S. Sampath, A.K. Sood, Solid State Commun. 150 (29-30) (2010) 1295–1298, https://doi.org/10.1016/j.ssc.2010.05.018.
[98] K.I. Bolotin, K.J. Sikes, Z. Jiang, M. Klima, G. Fudenberg, J. Hone, P. Kim, H. L. Stormer, Solid State Commun. 146 (9-10) (2008) 351–355, https://doi.org/10.1016/j.ssc.2008.02.024.
[99] F. Torrisi, T. Hasan, W. Wu, Z. Sun, A. Lombardo, T.S. Kulmala, G.-W. Hsieh, S. Jung, F. Bonaccorso, P.J. Paul, D. Chu, A.C. Ferrari, ACS Nano 6 (4) (2012) 2992–3006, https://doi.org/10.1021/nn2044609.